This is a peer-reviewed, accepted author manuscript of the following research article: Shittu, A. A., Abejide, S., Olisa, S. C., Mehmanparast, A., & Kolios, A. (2022). A stochastic framework for the assessment of horizontally curved aluminium bridge decks on steel girders. *Structures*, *42*, 125-143. https://doi.org/10.1016/j.istruc.2022.06.007

A stochastic framework for the assessment of horizontally curved aluminium bridge decks on steel girders

Abdulhakim Adeoye Shittu [ab*], Samuel Abejide[c], Samuel Chukwuemeka Olisa[d], Ali Mehmanparast[e], Athanasios Kolios[e]

[a]Faculty of Engineering, Federal University Wukari, 200 Katsina-Ala Road, Wukari P.M.B. 1020, Taraba State, Nigeria

[b]School of Water, Energy and Environment, Cranfield University, Bedford MK43 0AL, United Kingdom

[c]Civil Engineering Department, Walter Sisulu University, Butterworth Campus, 4960, South Africa

[d]School of Aerospace, Transport and Manufacturing, Cranfield University, Bedford MK43 0AL, United Kingdom

[e]Faculty of Engineering, University of Strathclyde, Glasgow G1 1XQ, United Kingdom

*E-mail address: adeoyeshittu@fuwukari.edu.ng (A.A. Shittu).

Abstract:

A purpose-developed structural reliability assessment (SRA) framework for the evaluation of horizontally curved aluminium alloy bridge decks on steel I-girders of centre subtended angle, $\theta \leq 34.4$ with precinct on the American Association of State Highway and Transportation Officials (AASHTO) load resistance factor design (LRFD) specification is presented. The finite element analysis (FEA) simulations were carried out in the ABAQUS© CAE in conjunction with the probabilistic assessment model developed using the First-order reliability method (FORM). Besides performing detailed design checks and a validation exercise, the developed SRA framework was used to examine the structural behaviour of the bridge assembly in the presence of stochastic design truck axle loads, structure's self-weight, among other loads whilst varying geometric properties. The most critical structural responses chosen at salient points obtained via FEA simulation is applied in deriving the limit state function (LSF), which is then substituted into the stochastic model within the purpose-developed iterative FORM algorithm to calculate the reliability index (RI), β of the structure. It is shown that the proprietary Alumadeck^{TM} system conforms with the LRFD specification, which stipulates that the target value of RI is 3.5 for resistance factor (RF) of 1.0 (assuming 80% composite action compression flange). The result also reveals that the RI shows a strong dependence on the composite action between the deck and the girder for RF of 1.0 full composite action (considering the failure of the bottom flange), indicating the safety index is within acceptable limits. Furthermore, it is revealed that the minimum composite action for safety is 40%, corresponding to a safety index of 1.16. Hence, it can be inferred from the foregoing that the Alumadeck^{TM} can withstand the stochastic axle load it is subjected to considering the HL 93 load design condition and satisfies all design criteria considered from a stochastic perspective based on the AASHTO LRFD guidelines, provided the minimum stiffner thickness $t_{stiffner}$ of $7mm$ is adopted (based on the FEA simulation results). A case study conducted herein established that the structural configuration selected (i.e. depth at $2.4m$, flange thicknesses at $21mm$, flange width at $50cm$ and web thickness at $16mm$) demonstrates the structural safety and durability of the bridge system coupled using the Alumadeck^{TM}.

Keywords: Structural reliability assessment (SRA), FORM, FEA, Alumadeck^{TM}, curved bridge decks

1 Introduction

Curved I-girder/ beam (CI-GB) bridges possess unique properties which enable them change direction within each span; making them ideal interchange structures for highways or to connect existing road sections where abutments cannot be relocated for physical or economic reasons (Ozgur 2007). Curved I-girder bridges in recent times are gaining widespread use as highway infrastructure as well as its use for; rebuilt atop existing structures to handle increasing traffic volumes or new interchange geometries within the context of urban settings (Linzell et al. 2010). CI-GB are most advantageous for constructing roadways in areas with serious geographical or manmade.

Majority of existing bridge decks are a subject of grief for engineers resulting from lack of innovative maintenance programs as well as alternative measures to mitigate failure. The conventional highway bridge deck system deteriorates over time due to changes in microclimate such as: variations in temperature gradient, moisture content fluctuation, freeze-thaw cycle and effect of alkaline minerals; usually a common problem with bridge structures. Corrosion of the reinforcing steel has been identified as the major cause of the deterioration in concrete; this still remains the most critical factor responsible for the large majority of structurally deficient bridges.

Most bridge decks require replacement after a cycle of 15 years minimum or after 20 years, depending on the design criteria, while the substructure and superstructure tend to last 40 years or more (Siwowski 2009b). Eventually, someday the bridge deck will need to be replaced. This has spirited the search for alternative decks that can resist environmental factors without any protective coating (Mazzolani 2006), reduce highway closure time and make retrofitting that meet the current design specifications possible while retaining the superstructure and substructure (Formisano et al. 2016).

Improving the design service life of bridges can be achieved using alternative materials, such as fibre-reinforced composites or aluminium. Since composites and aluminium are: lighter than steel and concrete, do not rust nor need painting or protective coatings, and have shorter fabrication as well as erection time; thus cheaper, they have a distinct advantage over other construction materials. aluminium will often be more affordable than concrete when whole-life costs are calculated. The suggestion made by Reynolds Aluminium Company (manufacturers of the Alumadeck^{TM}) has given way to a feasible alternative to conventional reinforced concrete decks. This deck is new and requires a close study of its characteristic structural behaviour.

Savings as high as 40% on steel material could be realised utilising an aluminium deck and steel girder system. These savings are attributed to the decrease in dead load that aluminium provides and the fact that the steel girders do not have to support large construction loads required during the curing of a reinforced concrete deck. Principally, because it is light, durable, and can be created into a wide variety of structural forms. These properties have been widely exploited in aerospace, railway carriage and architectural applications; they are also useful for bridgeworks. The low self-weight can be invaluable for handling during fabrication and construction and in the final design. The durability of aluminium alloys is very good, and it is one of the most underestimated virtues of the material. Most designers have often been confronted with negative perceptions – cost, corrosion, deflection and fatigue being the main concerns that abound. Many believe that aluminium alloys will not be fit for a highway bridge. In the main, these perceptions arise from examples of poor design. An aluminium structure will compete with any other material on cost with the right approach and will outperform most in service.

Consequently, when fabrication, erection and treatment costs are taken into account, there is little difference for the completed structure. Aluminium will often be cheaper than concrete when whole-life costs are calculated (Tindall 2008). Aluminium is the third most abundant element in the earth's crust, occurring mostly as aluminosilicates. The abundance of raw material and ease of recycling is such that resource depletion will not be an issue. It is extracted by electrolysis of alumina from bauxite fused with cryolite.

Structural analysis using the finite element method (FEM) has found a wide application for rigorous and accurate engineering response predictions and investigates structural behaviours difficult to experimentally study. Mathematical models used to evaluate the failure response of structures can either be one-dimensional (1-D) beam models or three-dimensional (3-D) finite element analysis (FEA) models. In most cases, the 3-D FEA mathematical models are more advantageous since they can analyse high-level stress distributions and predict structural responses more accurately. However, owing to the high fidelity, (3-D) FEA models have been widely applied to model similar structures as studied herein (Achmus and Abdel-Rahman 2005; Gentils et al. 2017; Kolios and Wang 2018; Wang et al. 2015, 2016b; c; Wang and Kolios 2017), and this study adopts the FEA approach to simulate these structural responses (Shittu 2020; Shittu et al. 2020d, c; a, 2021).

Stochastic finite element methods (SFEMs) have recently become an active area of research. As the name suggests, researchers in this field attempt to combine two crucial methodologies developed to deal with the complex problems of modern engineering: FEA and stochastic (or probabilistic) analysis. Stochastic analysis refers to the explicit treatment of uncertainties in any quantity entering the corresponding deterministic analysis at a specific period of time. The exact values of these quantities are usually unknown because they cannot be precisely measured (Breitung 2015; Papadopoulos et al. 2006). It describes the merging of advanced reliability methods with the FEM to obtain probability estimates for predefined performance criteria.

In order to apply the finite element (FE) technique, the region of interest is discretised by a FE mesh. The basic idea of the mean-based, second-moment analysis as used in stochastic FEA is to expand, via Taylor series, all the vector and the matrix stochastic field variables typical of deterministic FEM about the mean values of the random variables, to retain only up to second-order method terms and to use in the analysis only the first tier statistical moments. In this way, equations for the expectation and cross-covariance of the nodal displacement can be obtained in terms of the nodal displacement derivatives concerning the random variables (Beck and Gomes 2012). A comprehensive review of the capabilities and limitations of SFEMs has been discussed in (Shittu 2020; Shittu et al. 2020a). Given the drawbacks, such as this method being too intricate and computationally expensive, which could lead to fatal errors in programming such algorithms, a simple novel SFEM technique is developed herein, which offers a more efficient structural reliability assessment (SRA) framework capable of predicting the safety of engineering structures in a cost-effective time scale.

This study aims to investigate an integrated FEA and First Order Reliability Method (FORM) to ascertain the durability and safety levels of the proposed curved aluminium deck and the corresponding supporting curved steel I-girder under wheel loads. To achieve this aim, this is broken down into the following manageable steps: First to analyse the horizontally curved bridge deck using FEM for the system I and II stress, and second to obtain a suitable single equation based on the requirement of Ref. (AASHTO 2007, 2010) that will serve as the limit state function (LSF), next to perform a reliability evaluation of a horizontally curved bridge deck the system using the HL-RF FORM to determine the safety indices and last to propose apposite geometric dimensions. Having completed an extensive literature study (Ellingwood 2005; Ellingwood et al. 2014; Formisano et al. 2016; Guo et al. 2011; Imam et al. 2012; Kwon and Frangopol 2011; Li et al. 2016; Mazzolani 2006; Nie and Ellingwood 2005; Ren et al. 2021; Saydam and Frangopol 2013; Shittu 2015; Shittu et al. 2020a; Siwowski 2006b, 2009a; b; Thanapol et al. 2016; Wang et al. 2011b; Wang and Ellingwood 2015), to the best of the authors' knowledge, the work performed herein is the first study to the SRA of a complex curved bridge structural system employing a purpose-developed integrated FEA-FORM based SRA framework to evaluate the safety levels of the structure in terms of reliability index (RI), β. Structural designs employ the occurrence of infinite uncertainties as may arise during the service life of the component. Despite the common belief, many parameters of structural members' loading and load-carrying capacities are not deterministic quantities. Rather, they are random variables, and thus, optimum safety regarding safety index as stated in the design constraints cannot be achieved. In view of this, structures must be designed to serve their functions with a finite probability of failure (Nowak and Collins 2012).

Accumulation of research in bridge evaluation has indicated the justification of using reliability indices to measure safety (Ren et al. 2021). Reliability methods can be an important tool in evaluating existing or proposed structures (Melchers and Andre 2018) as the traditional component-based approach often does not reveal the actual load capacity (Nowak and Collins 2012).

The loads on a bridge at any time depend on many factors, such as the number of vehicles on the bridge, weight of the vehicle and the approach speed of the vehicles. The fact that we cannot ascertain the details about each vehicle passing over the bridge or the number of vehicles on the bridge at any time-space means that there are some uncertainties about the loads, the total load on a bridge and the bridge resistances (Nowak and Collins 2012). Given the anticipated uncertainties, there is a need to use a probabilistic approach (Wang and Ellingwood 2015) to evaluate the performance of the suggested aluminium alloy bridge deck in terms of strength characteristics and durability.

The remaining parts of this paper are structured as follows. Section 2 presents the theoretical background on bridge dynamics; Section 3 presents the methodology applied in the present study; Section 4 presents the results and discussion, followed by the conclusion in Section 5.

2 Bridge dynamics

Structural response of bridge components to dynamic and cyclic loading is critical to bridge evaluation. Structural resistance moments and serviceability depend on the load configuration. However, a bridge's actual service life response may be different from the initial loading configuration proposed. The actual load distribution characteristics and dynamic amplification of responses in a bridge have been studied using SRA, and this will be adapted for this study (A.O. et al. 2010; AASHTO 2010; Zureick and Naqib 1999).

Typically, analysis for vehicle- and wind-induced vibration is not to be considered in the bridge design. Although a truck crossing a bridge is not a static situation, the bridge is analysed by statically placing the truck at various locations along the bridge and applying a dynamic load allowance (DLA) as stated in AASHTO Specifications (AASHTO 2007). Due to the vertical bending and torsion coupling action. During construction, the non-composite steel girder must support the weight of the deck and steel weight in addition to other construction loads. There have been large relative deflections observed between girders on curved girder bridges during placement of concrete decks, making it challenging to maintain the specified final camber and superelevation and form and key in the construction joints (Zureick and Naqib 1999). The Alumadeck^{TM} is shop fabricated and, therefore, will not provide the same issues as reinforced concrete decks during construction.

2.1 Description of the bridge deck (Alumadeck^{TM})

Figure 1 refers to the two-dimensional view of an aluminium deck proposed for evaluation in this work. As shown in Figure 1(a) and (b), the Alumadeck^{TM} comprises the top and bottom surfaces and vertical and inclined stiffners.

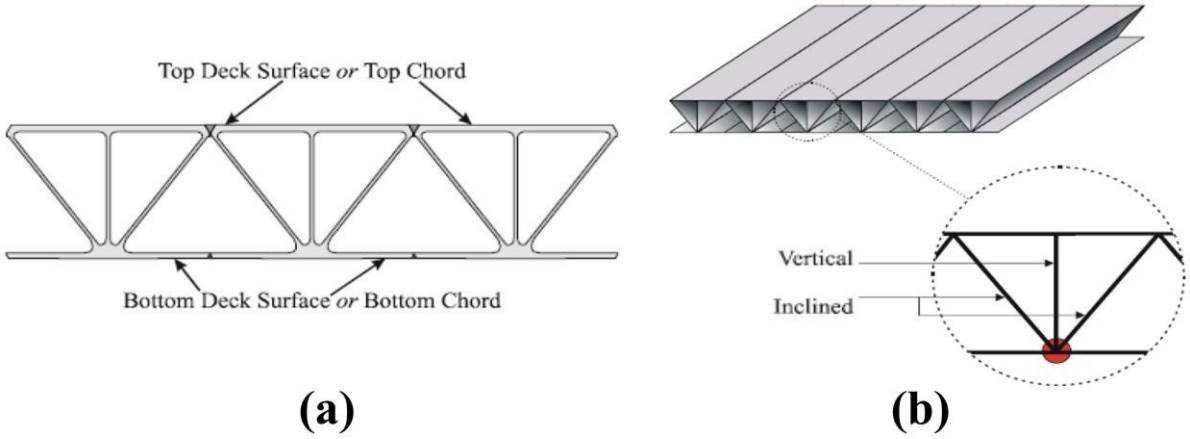

Figure 1. Nomenclature of: (a) top and bottom deck surfaces (b) stiffners (Siwowski 2009b).

2.2 Bridge design concepts

Research by Refs. (AASHTO 2010; BS5400-2 1978; Road Research 1979) have shown the types of loadings that act on bridges. The load-carrying capacity of bridges must meet two safety criteria, namely: unrestricted use by vehicles and restricted use by heavier vehicles. Two types of loads are considered in the design of bridges. First are the permanent loads known as the dead load, superimposed dead loads, loads due to filling materials, differential settlement, and loads due to creep and shrinkage. The dead load carried by a bridge member consists of its self-weight, portions of the superstructure's weight, and any fixed loads supported by the member. Secondly are transient loads defined as wind loads, temperature loads, exceptional loads, erection loads, centrifugal loads, braking, skidding and collision loads. The loadings used in this analysis are classified into dead loads and imposed loads. The imposed/ live load used is the HL-93 loading (AASHTO 2010). The load-deformation of a curved plate is influenced by the flexural and torsional rigidities of the slab and loadings. These deformations are expressed in the mathematical form of differential equations. The differential equations of flexure for curved orthotropic plates are expressed relative to the radius and angle of rotation with other stiffness parameters like modulus of elasticity and rigidity, moments of inertia and torsional constant.

2.2.1 Dead Loads

According to Ref. (AASHTO 2010), the dead load includes the weight of all structural components, appurtenances and utility, earth cover, future overlays, and planned widening. Dead loads are sub-divided into three categories: A dead load of structural components (DC) divided into the weight of the aluminium deck, DC 1, and weight from barriers, medians, and sidewalk/weight of parapets acting on the composite structure, DC 2. Future wearing surface (FWS) loads are considered DW loads.

2.2.2 Live Loads

The live loads of interest in this research are the AASHTO design vehicular live loads with the appropriate DLA, multiple presence factors and centrifugal forces evaluated in this work. Braking forces and vehicular collision forces are neglected due to their anticipated small effect on the bridge responses. Additionally, according to the provisions of Ref. (AASHTO 2007), the effect of superelevation can be neglected for superelevation angles between 0% and 10% (zero and ten per cent). Therefore, the effect of superelevation is neglected. Since the bridge is horizontally curved, the effects of centrifugal force must be considered. Centrifugal force is a radial force applied above the deck, transferred through the vehicle's wheels to the deck. Since centrifugal force is applied above the deck, it creates an overturning moment. As a result, the overturning moment tends to increase the vertical wheel forces towards the outside of the bridge and decrease them towards the inside of the bridge. The same author elucidates further advanced information regarding this, such as the HL-93 design truck or tandem load with dynamic allowance, design lane load without dynamic allowance, etc., in Ref. (Shittu

2015). The truck loading, as well as centrifugal loads, also considered herein, of interest, is described below:

2.2.3 Truck Loading

The total weight of the design truck is $35.58 + 142.34 + 142.34 = 320.25$ kN. Including 33% impact, $1.33 \times 320.25 = 425.94$ kN. For four (4) trucks, including the multiple presence factor, m: $4(425.94)(0.65) = 1{,}107.4$ kN and total live Load = $891.7 + 1107.4 = 1999.1\ kN$.

2.2.4 Load Application

The rules for applying the AASHTO (AASHTO 2010) loadings are given as follows: (1) The loading or standard truck loading shall be assumed to occupy a width of $3.0m$. These loads shall be placed in $3.3m$ wide design traffic lanes spaced across the entire bridge roadway width in numbers and positions required to produce maximum stress (2) Each $3.0m$ lane loading or single standard truck shall be considered as a unit, and fractional values for lane loading or trucks shall not be used (3) AASHTO allows for a reduction in maximum stress that is produced in any member by loading any number of traffic lanes simultaneously. For one or two lanes, 100%; Three lanes, 90%; Four or more lanes, 70%.

2.2.5 Centrifugal Load

The design speed is 40 mph ($64.4\ km/hr$). The centrifugal force coefficient is given by: $\mathrm{C} = \left(\frac{4}{3}\right)\frac{\mathrm{V}^2}{\mathrm{gR}}$, where: C = coefficient to compute centrifugal force, V = highway design speed, m/s, g = gravitational acceleration, 9.81 m/sec^2, R = radius of curvature of the traffic lane, m, the design speed in m/s = 40 mph/0.628 = 18 m/sec, $\mathrm{C} = \left(\frac{4}{3}\right)\frac{(18)^2}{(9.81)(182.88)} = 0.24$. This is applied to the truck axle loads only, without the DLA, and with the factor, m. The centrifugal force for four trucks is $4(320.26\ kN)(0.24)(0.65) = 199\ kN$. For the design of bridges, both the truck and lane loading are to be considered, and the one which yields the worst effect should be adopted. In the case of truck loading, only one truck is considered for each traffic lane for the whole of its length. There is no reduction in load intensity for up to two lanes of traffic loaded lanes.

2.3 Load Combination

Two load combinations are considered in this study: (1) The strength I loading combination:

$$25\ DC1 + 1.25\ DC2 + 1.5DW + 1.75(LL + IM + CE + BR) + 1.2(TU), \quad (1)$$

and (2) strength II:

$$1.0DC1 + 1.0DC2 + 1.0DW + 1.33(LL + IM + CE + BR) + 1.2\ (TU), \quad (2)$$

Where LL represents the vehicular live load, which covers for IM the vehicular DLA, CE the vehicular centrifugal force, BR the vehicular braking force, and TU uniform temperature.

2.3.1 Bride load model

The load model applied in this research are the dead and live load component derived from AASHTO (AASHTO 2010) specifications. The dead load components employed include factory made member weight (girders), deck slab and wearing coarse. Live load parameters are derived from AASHTO (AASHTO 2010), designated as HL-93. The models used considered various positions for both single and multiple lane loads to obtain maximum moment on the deck for transverse truck locations. Figure 2 shows the truck location, which is $0.15m$ close to the center line (A.O. et al. 2010).

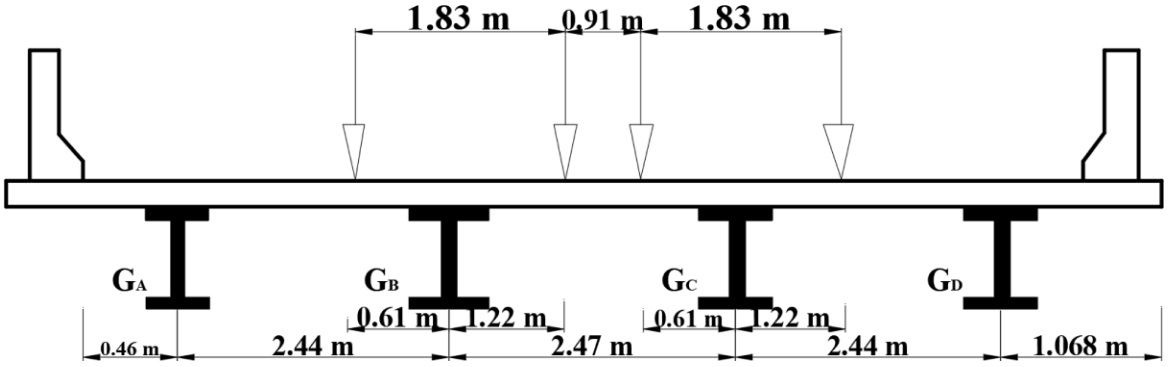

Figure 2. Typical transverse section of the bridge showing HL-93 loading location (AASHTO 2010).

2.3.2 Bridge deck design

According to AASHTO (AASHTO 2010), the first principle design of a bridge deck slab is perpendicular to the centre line of traffic (direction of vehicular loading). The deck slab is considered a continuous and simply supported beam in the transverse direction. This assumption is based on an alternative method of analysis for determining the maximum moment. This method of analysis is utilised to determine the lateral live-load distribution on the bridge girders. Although, lateral live-load distribution factors rely on varied environmental load configurations. There is a need to assess specific ranges of applicability for the use of approximate methods of analysis. Therefore, extending the application of such approximate methods beyond the limits requires sound and reasonable judgement. Otherwise, an advanced analytical approach should be adopted. The basic partial differential equations governing the behaviour of a curved plate are derived on the assumptions that external loads are normal to the surface of the deck plate, that the plate acts as a monolithic unit, that the deck plate is homogenous, isotropic and elastic, that the plane surface initially perpendicular to the middle surface of the deck plate remains plane and perpendicular to the middle surface during bending, and that the deflections are small in relation to the thickness of the orthotropic plate. Ref. (Heins and Hails 1969) showed that the reactions and deflections were dependent on the flexural and torsional properties of the plates. Analysis of a curved plate or girder can be done by the solution to the partial differential equation using finite difference, finite element and slope deflection method.

2.3.3 Curved beam design

Ref. (Heins 1975) derived charts for curved beams, which can be used to determine the forces. The equations used from the charts can be expressed as:

$$M_{radial} = M_{straight}K_1K_2K_3, \text{ where: } F_{radial} = F_{straight}K_1K_2K_3, \qquad (3)$$

where K_1 represents the amplification factor, K_2 the distribution factor and K_3 the reduction factor. For the moments: $K_1 = \frac{0.15}{n} \times \frac{L}{R} = 1.0$; where, $K_2 = \frac{0.4L(n+3)}{R} + 0.6 = 1.0$; and $K_3 = 1.0$, Therefore, since we are dealing with a single span, then $n = \frac{R^2}{100}$; considering shear, $K_1 = 1.0$, $K_2 = \frac{0.4L(n+3)}{R} + 0.6 = 1.0$; and $K_3 = 1.0$ (i.e. a single-span case). Again $K_1K_2K_3 = K$, which can be expressed as $K = 0.078\theta + 0.669$ where θ is the angle subtended by the girders in radians. The greater of the K values obtained is used in the design.

2.3.4 The AASHTO flexural resistance equations

It is crucial to recall the structural mechanics' expression as this will be extensively applied herein:

$$\sigma = \frac{Mc}{I} \qquad (4)$$

where σ represents stress, M the bending moment, c the distance to the structural element's neutral axis along the height of the cross-section, and I is the centroidal moment of inertia.

The AASHTO (AASHTO 2007) flexural resistance equations that address the combined effects of major-axis bending and flange lateral bending are:

$$f_{bu} + \frac{1}{3} f_l \leq \phi_f F_n, \tag{5}$$

while for members in which the flexural resistance is expressed in terms of stresses and

$$M_u + \frac{1}{3} f_l S_x \leq \phi_f M_n, \tag{6}$$

whilst for members in which the flexural resistance is expressed in terms of moments, where: f_{bu}= flange major-axis bending stress, f_l= flange lateral bending stress, $\phi_f F_n$= factored flexural resistance in terms of the major-axis bending stress, M_u= member major-axis bending moment, S_x=elastic section modulus about the major-axis of the section to the flange under consideration taken as $\frac{M_{yf}}{F_{yf}}$, and $\phi_f M_n$ = factored flexural resistance in terms of member major-axis bending moment. The plastic moment capacity is given by:

$$M_p = \frac{P_w}{2D}[\bar{y}^2 + (D - \bar{y})^2] + P_s d_s + P_c d_c + P_t d_t \tag{7}$$

where, $P_s = f_s A_s$; $P_c = f_{yc} A_{fc}$; $P_t = f_{yt} A_{ft}$; $P_w = f_{yw} A_w$; $\bar{y} = \frac{D}{2}\left(\frac{P_t - P_c - P_s}{P_w} + 1\right)$; $d_s = \frac{t_{slab}}{2} + t_{haunch} + Y_{bar}$; and $d_c = Y_{bar} - \frac{t_{fc}}{2}$; $d_t = D - \bar{y} + \frac{t_{ft}}{2}$. Again, $D_p = Y_{bar} + t_{slab} + t_{haunch}$; $D = D + t_{haunch} + t_{slab} + t_{ft}$. In addition, $M_n = M_p$ if $D_p \leq 0.1D_t$; otherwise, $M_n = M_p\left(1.07 - \frac{0.7D_p}{D_t}\right)$.

where f_s= slab bending stress, A_s= effective area of the slab, f_{yc}= yield stress of the compression flange, A_{fc}= effective area of compression flange of the girder, f_{yt}=yield stress of the tension flange, A_{ft}= effective area of tension flange of the girder section, f_{yw}=yield stress of the web of the girder, A_w= area of web of the girder section, P_n= respective force, $\bar{y}$= centroid of the composite section (i.e. girder plus haunch plus Alumadeck^{TM}), t_{slab}= thickness of the Alumadeck^{TM} slab, t_{fc}= thickness of compression flange, t_{ft}=thickness of tension flange and t_{haunch}= thickness of haunch.

The proposed aluminium deck on steel girders is evaluated using FEM and SRA, and the formulations of AASHTO (AASHTO 2007, 2010) with parameters such as stiffner thickness, percentage composite action, etc., are studied herein to determine the possibility of use in horizontal curves and sometimes in skewed situations whilst the safety of doing this is also evaluated. The methodology employed is discussed in the next Section.

3 Methodology

3.1 Structural reliability

Complex engineering structures are designed in accordance to limit state (LS) methods. Serviceability and ultimate LS service life parameters being the two primary criteria for analysis makes the structures unfit for their intended purpose once exceeded. Ample experience in the past and recent times has shown that unique designs or unfamiliar constructional methods and materials increase the risk of failures.

Over the years, structural system design has assumed that all loads and strengths are deterministic. The strength of an element was determined so that it exceeded the load with a certain margin. The ratio between the strength and the load was denoted as the safety factor. This number was considered as a measure of the reliability of the structure. In codes of practices for structural systems, values for loads, strengths and safety factors are prescribed. These values are traditionally determined based on experience and engineering judgment. Hence, structural analysis and design have traditionally been based on deterministic methods. However, uncertainties in the loads, strengths, and modelling of the systems require that methods based on probabilistic techniques have to be used (Ditlevsen and Madsen 2007; Ellingwood et al. 2014; Ghosn et al. 2016). Engineering design is usually a trade-off between

maximising safety levels and minimising cost. In comparison, deterministic safety factors do not provide adequate information to achieve optimal use of the available resources to maximise safety, while the probabilistic analysis does (Melchers and Andre 2018; Shittu et al. 2021; Wang et al. 2011a; Wang and Ellingwood 2015). Probabilistic analysis method of design provides detailed information regarding the behaviour of the structural member as well as response to the structural member under variable loading.

Sorensen (Sorensen 2003) defined the reliability of structural systems as the probability that the structure under consideration has a proper performance throughout its lifetime. This could be defined as the structure's ability to fulfil its design purpose for some specified reference period (Choi et al. 2006; Shittu 2020). Computer techniques of structural analysis have improved the accuracy of representing the actual behaviour of bridge components. Advanced programs (e.g. ABAQUS, NASTRAN, ANSYS) are available for linear and non-linear analysis of complex structural systems. The reader is referred to Ref. (Shittu 2015) for further detailed explanation on the need for SRA in the design of bridges.

The study of structural reliability is concerned with calculating and predicting the probability of a LS violation for engineered structures at any stage during their life. In particular, the study of structural safety concerns the violation of the ultimate or safety LS for the structure. The "violation" of an LS is the attainment of an undesirable condition for the structure, i.e. damage to a part of the structure or total collapse of the structure, which could lead to loss of human lives (Melchers and Andre 2018).

3.1.1 Resistance and load interaction

Basic design standards in reliability methods permit consideration allowance to the effect of a load (S) and the resistance (R) offered by the structure. Although, the load (ultimate moment) and resistance moment, S and R, can be described by a known probability density function $F_s(\cdot)$ and $F_R(\cdot)$, respectively. The structural load can be obtained from the applied loading via the maximum moment generated. In most cases, the assumption ensures that R and S are expressed in the same unit.
Considering only the safety of a structural element, a structural element has failed if its resistance - R, is less than the stress resultant - S acting on it. The probability of failure (POF), P_f of the structural element can be expressed in any of the following ways:

$$P_f = P(R - S), \tag{8}$$

Where R= strength (resistance) and S= loading in the structure. The failure, in this case, is defined in the region where R-S is less than zero, or R is less than S, that is:

$$P_f = P(R - S) \leq 0. \tag{9}$$

As an alternative approach to Equation (8), the POF can also be given as:

$$P_f = P\left(\frac{R}{S} \leq 1\right) \tag{10}$$

wherein this case, the failure is defined in the region where $P_f$is less than one, or R is less than S, which is $P_f \leq 1$ or $R < S$. It could also be expressed as

$$P_f = P(\ln R - \ln S \leq 1) \tag{11}$$

or in general,

$$P_f = P[G(R, S) \leq 0] \tag{12}$$

where G(x) is the LSF, and the POF is identical with the probability of the LS violation. For any random variable X, the cumulative distribution function $F_X(x)$ is given by:

$$F_x(x) = P(X \leq x) = \int_{-\infty}^{x} f_x(y)dy \tag{13}$$

Provided that $x \geq y$, it follows for the common, but a particular case where R and S are independent, the expression for the POF is:

$$P_f = P(R - S \leq 0) = \int_{-\infty}^{\infty} F_R(x) f_s(x) dx \quad (14)$$

Expression (14) is known as the "convolution integral" and $F_R(x)$ is the probability that $R < x$, or the probability that the actual resistance R of the member is less than some value x.f_s(x) represents probability that the load effect S acting in the member has a value below x and x + Δx in the limit as $\Delta x \to 0$. Considering all possible values of x, total failure probability is obtained as follows:

$$P_f = \int_{-\infty}^{\infty} [1 - F_s(x)] F_R(x) dx \quad (15)$$

i.e., the sum of all the cases of resistance for which the load exceeds the resistance.

3.1.2 Limit State Functions (LSF)

When applying probabilistic evaluation methods in structural engineering, it is essential to define performance criteria, which can be achieved via the LSFs. In SRA, the term 'failure' denotes the event of not meeting performance criteria. Limit states are the boundaries between safety and failure. In bridge structures, failure can be defined as the inability to carry traffic. Bridges can fail in many ways (modes of failure), by cracking, corrosion, excessive deformations, exceeding carrying capacity for shear or bending moment, local or overall buckling, and so on. Members can fail in a ductile or brittle manner. In the traditional approach, each mode of failure is considered separately. There are three types of limit states. Ultimate limit states (ULS) are mostly related to the bending capacity, shear capacity and stability. Serviceability limit states (SLS) are related to gradual deterioration, user's comfort or maintenance costs. For further details, see Ref. (Nowak 2004).

According to Refs. (Shittu 2020; Shittu et al. 2020b; d), the ULS (ultimate limit state) defines the ability of the structure to resist yielding. In terms of the ULS, the maximum stress in the support structure $\sigma_{VM,max}$ should not exceed the allowable stress limits $\sigma_{VM,allow}$. The LSF for the Von Mises criterion can be expressed as follows:

$$g_u(x) = \sigma_{VM,allow} - \sigma_{VM,max} \quad (16)$$

The allowable stress $\sigma_{VM,allow}$ can be expressed as follows:

$$\sigma_{VM,allow} = \frac{\sigma_y}{\gamma_m} \quad (17)$$

where σ_y is the yield strength, and γ_m is the material safety factor. This concept will be applied later in this study.

3.2 First-Order Reliability Method (FORM)

FORM is an efficient tool used to assess the structural reliability of elements. FORM provides means for calculating the partial safety factors regarding allowable load variations that a structural member can sustain during its design life. FORM makes use of both analytical and approximation methods and comprises three stages. Firstly, independent of whether each parameter has been defined as Normal, Log-Normal or Gumbell distribution, all variables are first transformed into equivalent standard space with zero mean and unit variance.

The original limit state surface (LSS) is then mapped onto the new LSS. Secondly, the shortest distance between the origin and the LSS, termed the reliability index (RI), β is evaluated; this is termed the design point, or point of maximum likelihood, and gives the most likely combination of basic variables

to cause failure. Finally, the failure probability associated with this point is then calculated. FORM can be easily extended to non-linear limit states and has a reasonable balance between ease of use and accuracy (Webster and Bannister 2001).

In brief, having determined the stochastic variables and obtained the performance function, the RI, β in this study, is then calculated using the iterative Hasofer Lind Rackwitz-Fiessler (HL-RF) FORM. This method incorporates a number of uncorrelated standard normal random variables. The original variables, which may, in general, be correlated and non-normal, are transformed to the u-space using well-established transformations such as the Rosenblatt's transformation. The exact failure probability is the integral of the joint probability density function over the failure domain $g(u) < 0$. The first-order Taylor series expansion of the LSS $g(u) = 0$ is applied at the point with the shortest distance from the origin in the u-space. An RI, β can be referred to as the shortest distance from the origin to the LSS in this space. The point of which the distance from the origin is minimum to the limit-state surface denotes the worst combination of random variables and is thus called the design point or most probable failure point (MPP). The HL-RF algorithm can be employed in recursively searching for the MPP. This technique allows the algorithm to accommodate a wide range of probabilistic distribution functions. Further advanced explanation on the principles is elucidated in the next Subsection.

3.3 Concept of FORM

Having defined the LSF $g(u_1, \ldots, u_n)$ in the u-dimensional Euclidean space, the FORM aims to approximate the failure domain $F = \{\boldsymbol{u};\ g(\boldsymbol{u}) < 0\}$ by a halfspace by replacing the LSF by a linear tangent hyper-plane at the point $\boldsymbol{u}^*$**.** The LSS $G = \{\boldsymbol{u};\ g(\boldsymbol{u}) = 0\}$ has the nearest geometric distance to the origin, which means that the PDF is maximal there since it is proportional to $-|\boldsymbol{u}|^2$. The HL-RF algorithm revolves around finding a point $\boldsymbol{u}^*$ for an LSF $g(\boldsymbol{u})$ at the normal standard space such that

$$|\boldsymbol{u}^*| = \min_{g(\boldsymbol{u})=0} |\boldsymbol{u}| = \min_{g(\boldsymbol{u})\leq 0} |\boldsymbol{u}| \qquad (18)$$

i.e. with the shortest distance to the origin. Basically, this involves linearising the LSF at an initial point, calculate the design point for the linearised LSF and then proceed recursively, always again linearising until convergence is achieved. Further advanced information on this concept can be found in (Shittu et al. 2020a). See Figure 3 as follows:

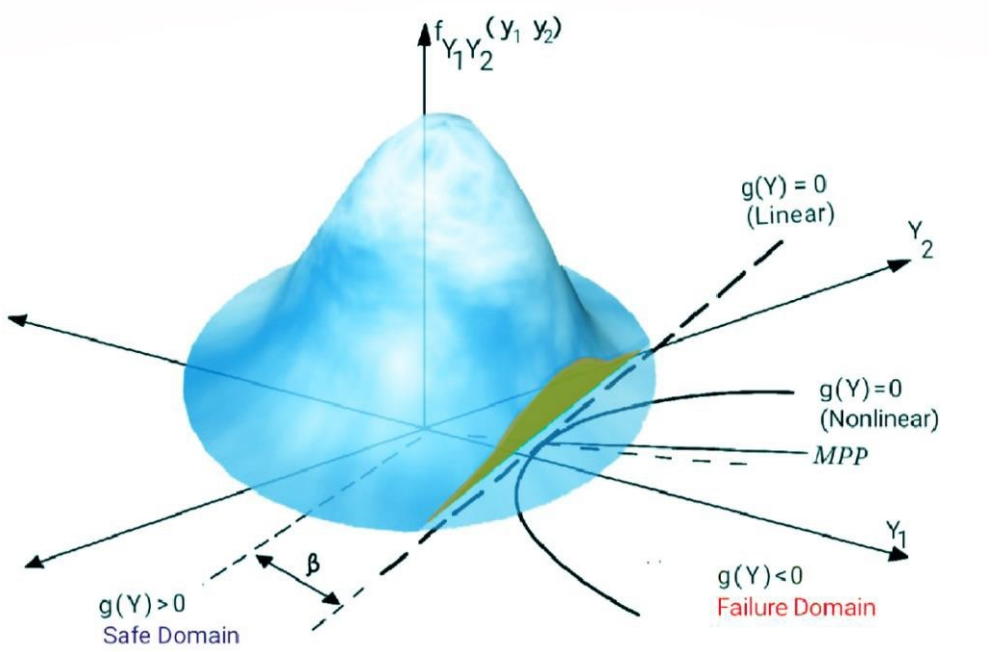

Figure 3. Illustration of the First-order reliability methods (FORM) approximation. See Ref. (Shittu et al. 2020a) for more details.

3.4 Theory of curved decks

According to Refs. (Heins and Hails 1969; Timoshenko and Woinowsky-Krieger 1982), the differential equation (DE) for flexure of a curved plate is given as:

$$D_r\frac{\partial^4\eta}{\partial r^4} + 2H\frac{\partial^4\eta}{r^2\partial r^2\partial\theta^2} + D_\theta\frac{\partial^4\eta}{r^4\partial\theta^4} + 2D_r\frac{\partial^3\eta}{r\partial r^3} - 2H\frac{\partial^3\eta}{r^3\partial r\partial\theta^2} - D_\theta\frac{\partial^2\eta}{r\partial r^2} + 2(D_\theta + H)\frac{\partial^2\eta}{r^4\partial\theta^4} + D_\theta\frac{\partial\eta}{\partial r^3\partial r} = q \quad (19)$$

where the parameters D_r, D_θ and H is the stiffness parameters expressed as

$$D_r = \frac{Et^3r}{[12(1-\mu^2)]} \quad (20)$$

$$D_\theta = \frac{Et^3r}{[12(1-\mu^2)]} \quad (21)$$

$$H = GK_1 \quad (22)$$

$$D_{r\theta} = H/2 \quad (23)$$

where, P = loading, r = radius of bridge, E = modulus of elasticity, K_1 = torsional constant, μ = Poison constant, t = thickness of deck, r = unit radius of deck, G = modulus of rigidity, θ = angle subtended by section, η = deflection of the section, q = uniformly distributed load; $D_{r\theta}$ = torsional rigidity; D_r = flexural rigidity in the r-direction; D_θ = flexural rigidity in the θ direction. The general solution to Equation (19) determined by Ref. (Heins and Hails 1969) can be expressed as:

$$\eta = \sum[AX^{m1} + BX^{m2} + CX^{m3} + DX^{m4}]\sin\lambda\theta + \frac{4pr^4\sin\lambda\theta}{D_r n\pi[72 - 18\beta\lambda^2 - \alpha(8 + 2\lambda^2 - \lambda^4)]} \quad (24)$$

where, $\alpha = \frac{D_\theta}{D_r} = 1$, $\beta = \frac{H}{D_r} = 0.98$, $\lambda = \frac{n\pi}{\theta} = 0.37$, $X = \frac{r_i}{r}$ in which the four roots of the equations m_1, m_2, m_3, and m_4 can be expressed as:

$$m_1, m_2, m_3, m_4 = \pm\{(\alpha + 2\beta\lambda^2 + 1)/2 \pm [0.25(1 + \alpha^2\beta^2)^2 - (\lambda^2 - 1)^2\alpha]^{\frac{1}{2}}\}^{\frac{1}{2}} + 1 \quad (25)$$

where for the above Equation, $X = \frac{r}{r_\theta}$, r = radius at the point of consideration, r_θ = radius of the bridge deck system. The curved plate moment DEs are as follows:

$$M_r = -D_r\left(\frac{\partial\eta}{\partial r^2}\right) \text{ (Radial Moment)} \quad (26)$$

$$M_\theta = -D_r\left(\frac{\partial\eta}{r\partial r} + \frac{\partial\eta}{r^2\partial\theta^2}\right) \text{ (Angular Moment)} \quad (27)$$

$$R_r = \left[\left(\frac{\partial^3\eta}{\partial r^3} + \frac{\partial^3\eta}{\partial r^2}\right) + 2\frac{H}{D_r}\left(\frac{\partial^3\eta}{r^3\partial r\partial\theta^2} - \frac{\partial^3\eta}{r^3\partial\theta^2}\right) - \frac{D_\theta}{D_r}\left(\frac{\partial^3\eta}{r^3\partial r} + \frac{\partial^3\eta}{r^3\partial\theta^2}\right)\right] \quad (28)$$

(Radial Shear)

$$R_\theta = -D\left[\left(\frac{\partial\eta}{r^2\partial r\partial\eta} + \frac{\partial^3\eta}{r^3\partial r\partial\theta}\right) + 2\frac{H}{D_\theta}\left(\frac{\partial\eta^2}{r^2\partial r\partial\theta} + \frac{\partial\eta}{r^2\partial r\partial\theta} + \frac{\partial\eta}{r^3\partial r}\right)\right] \quad (29)$$

(Angular shear)

Equations (26) and (26) are expressed in terms of the general solution of Equation (24) for the radial moment and radial shear. Since the angular moment and shear are much smaller than the radial moment and shear, the angular moment and shear shall be neglected. Thus,

$$-M_r \frac{r^2}{D_r} = [[(Am_1(m_1-1))X^{m1} - Bm_2(m_2-1)X^{m2} + Cm_3(m_3-1)X^{m3} + Dm_4(t)X^{m4}]] \sin\lambda\theta, \quad (30)$$

and

$$-R_r \frac{r^3}{D_r} = [[Am_1(m_1-1)^2 - 2\beta\lambda^2(m_1-1) - \alpha(m_1-\lambda^2)]X^{m1} + [Bm_2(m_2-1)^2 - 2\beta\lambda^2(m_2-1) - \alpha(m_2-\lambda^2)]X^{m2} + [Cm_3(m_3-1)^2 - 2\beta\lambda^2(m_3-1) - \alpha(m_3-\lambda^2)]X^{m3} + [Dm_4(m_4-1)^2 - 2\beta\lambda^2(m_4-1) - \alpha(m_4-\lambda^2)]X^{m4}] \sin\lambda\theta \quad (31)$$

The above concept will be applied in herein in the upcoming Section 4. The flowchart of the developed SRA framework for this study is depicted in Figure 4.

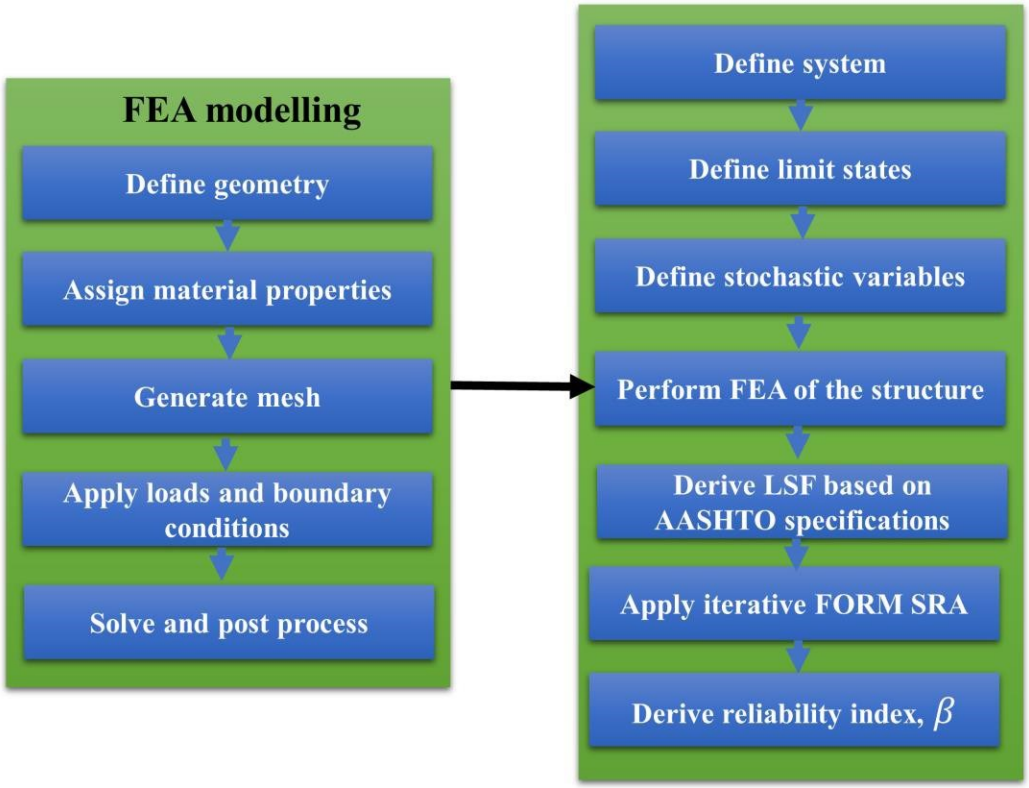

Figure 4. Flowchart of the purpose-developed SRA framework. Adapted from: Refs. (Shittu 2020; Shittu et al. 2020d; a).

4 Results and discussion: FEA, design and stochastic optimisation

4.1 FEA results

The FEA results to calculate the critical structural responses, the maximum displacement, $U_{max}\,(mm)$ and maximum critical stress kN/m^2 employing the system I and II stress (i.e. the bending of the deck between girders) concept is presented in this Subsection. The system II stress option is adopted because it examines the deck behaviour on a local scale. Therefore, this will enhance the calculation of the

structural response of interest using the various AASHTO limit state design criteria. The structural behaviour of the deck was studied while varying salient applied normal and centrifugal stresses at various geometric properties.

4.1.1 FEA modelling on ABAQUS©

The deck was analysed using FEA software ABAQUS©. Figure 5(a) depicts the part; the case study considered - a horizontally curved aluminium alloy deck - Alumadeck^{TM} – radius = $100m$, Subtended angle = $34.4°$ while Figure 5(b) shows the 3D zoomed display of vertical and inclined stiffners. The mesh generated was selected taking into account of trade-of between computational cost and precision.

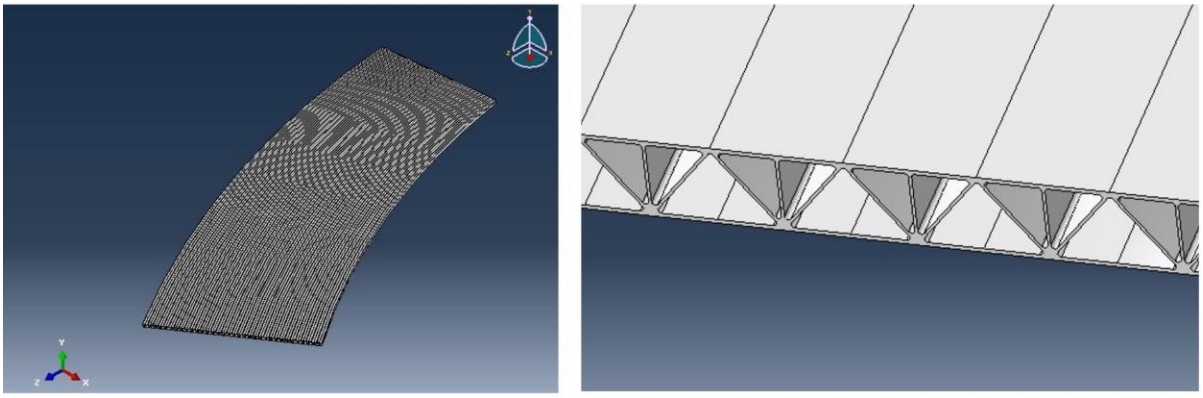

(a) **(b)**

Figure 5. The developed horizontally curved bridge deck model in the ABAQUS© environment: (a) Built 3-D model (b) 3-D display of the vertical and inclined stiffners[1].

As these Figures depicts, the Alumadeck^{TM} and the section as built in ABAQUS© is elucidated (i.e. see vertical and inclined stiffners as modelled therein). The solid element feature in ABAQUS© configuration settings was adopted. The material properties of the Alumadeck^{TM} were assigned in the model: (1)The Young's Modulus assigned was $68.9GPa$, and the Poison's ratio was 0.33. (2)The density and the yield stress were also assigned. The loading configurations entered into the model applied on the deck is according to HL-93 load AASHTO specifications.

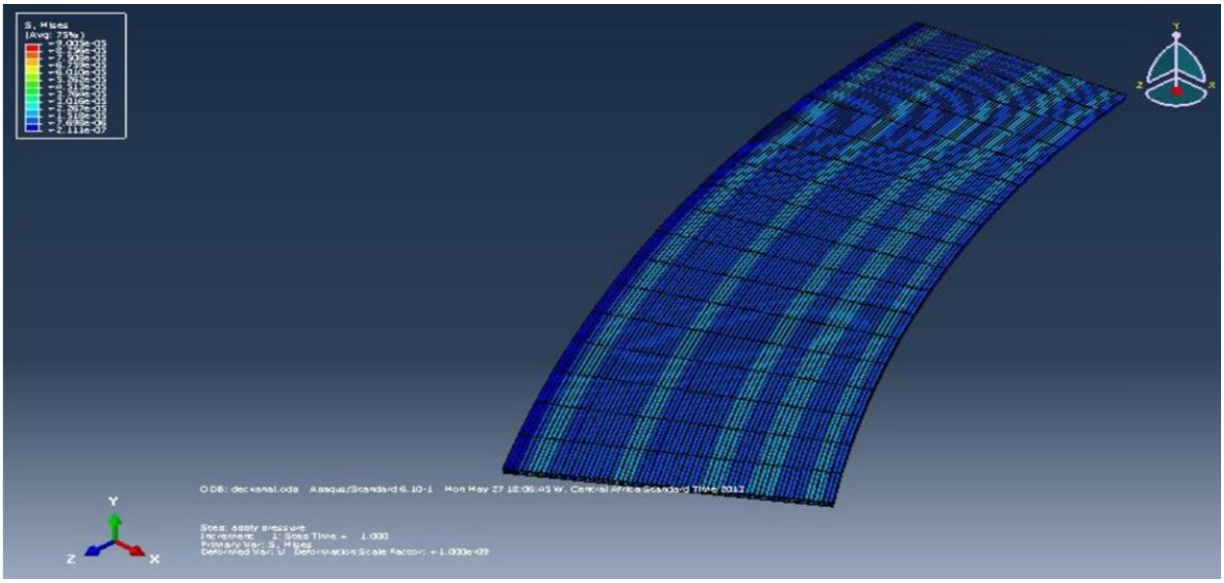

Figure 6. 3D ABAQUS© model result display of the contours of Von Mises stress

[1] The structural model developed in ABAQUS© is as depicted in white grey colour

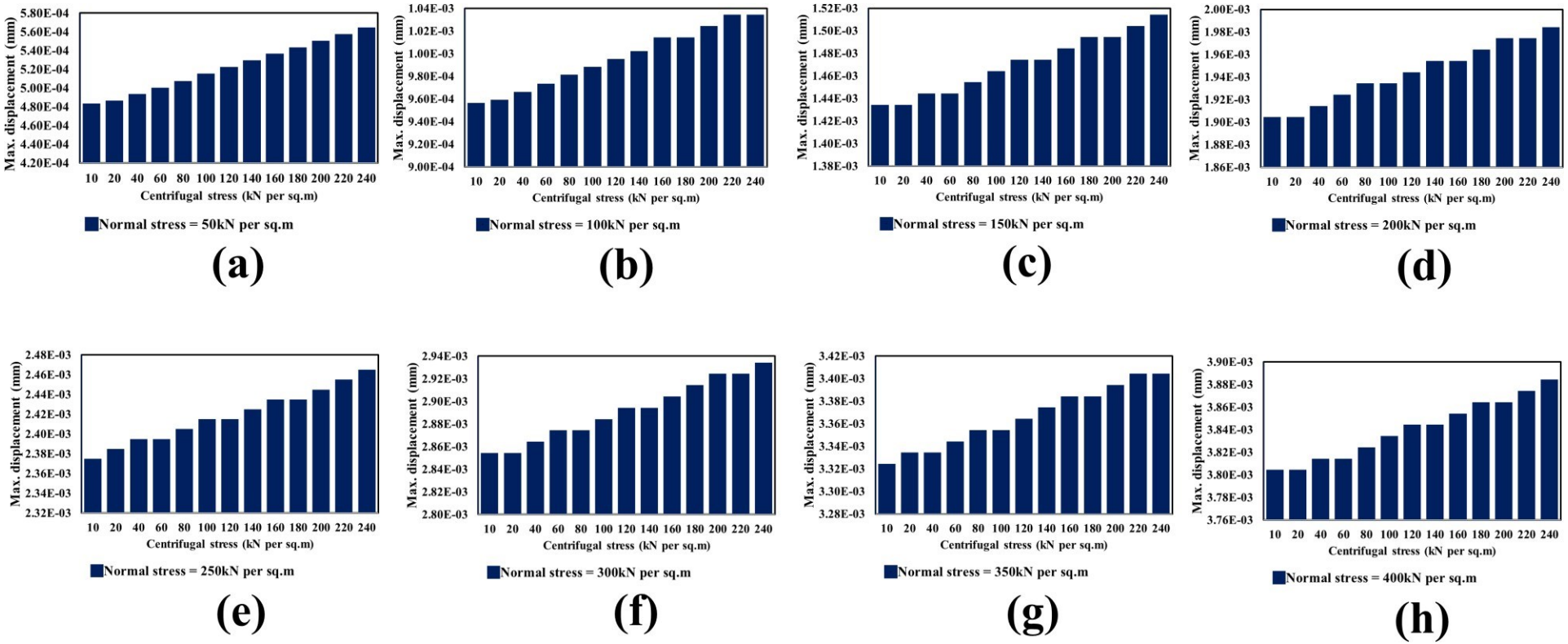

Figure 7. Variation of maximum displacement ($\boldsymbol{mm}$) against centrifugal stress ($\boldsymbol{kN/m^2}$) – $\boldsymbol{t = 5mm}$

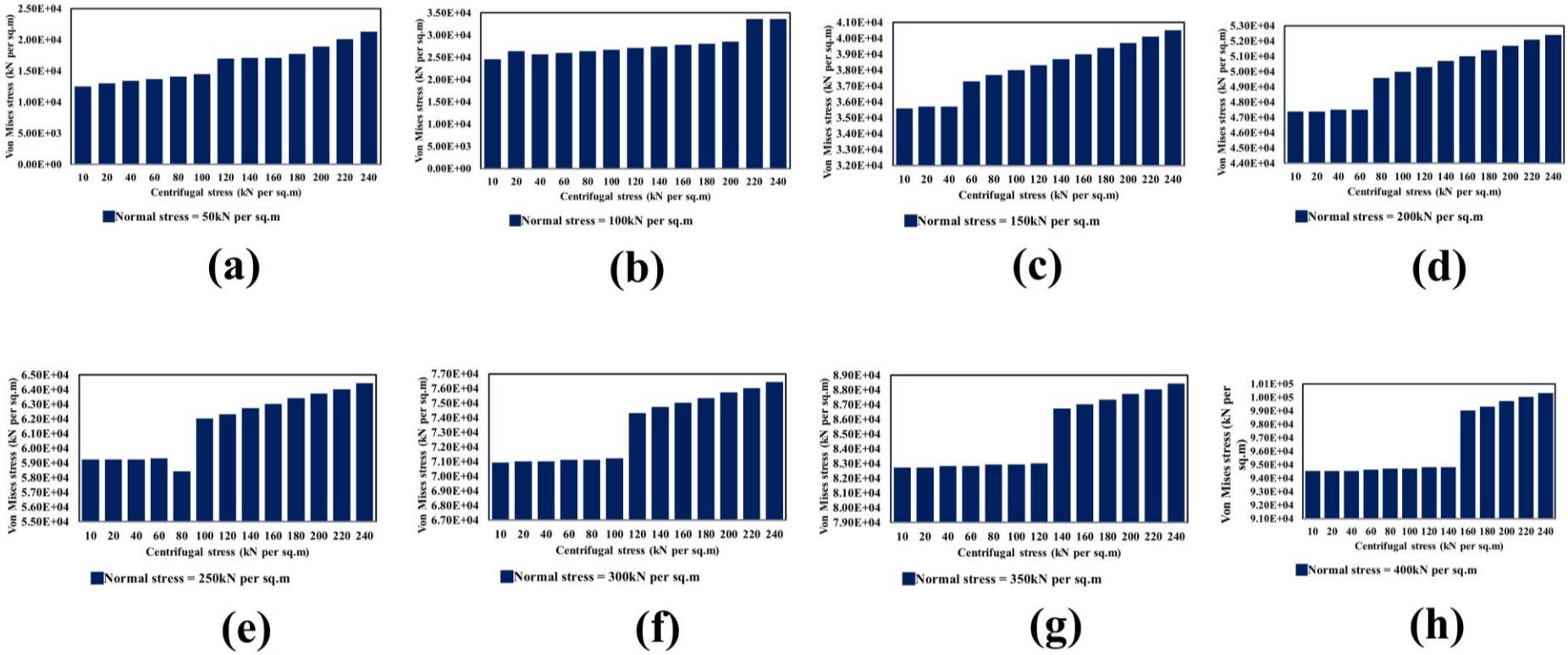

Figure 8. Variation of maximum Von Mises stress ($\boldsymbol{kN/m^2}$) against centrifugal stress ($\boldsymbol{kN/m^2}$) - $\boldsymbol{t = 5mm}$

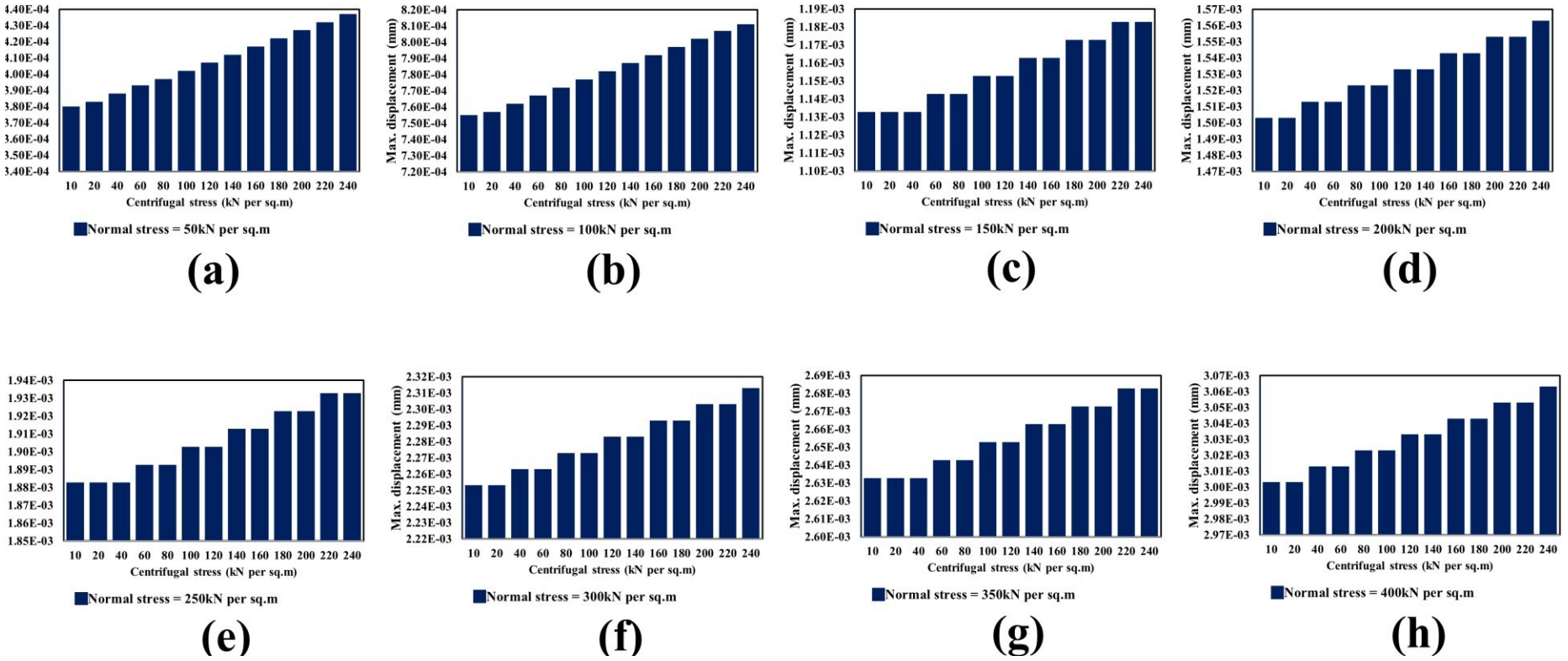

Figure 9. Variation of maximum displacement ($\boldsymbol{mm}$) against centrifugal stress ($\boldsymbol{kN/m^2}$) - $\boldsymbol{t = 7mm}$

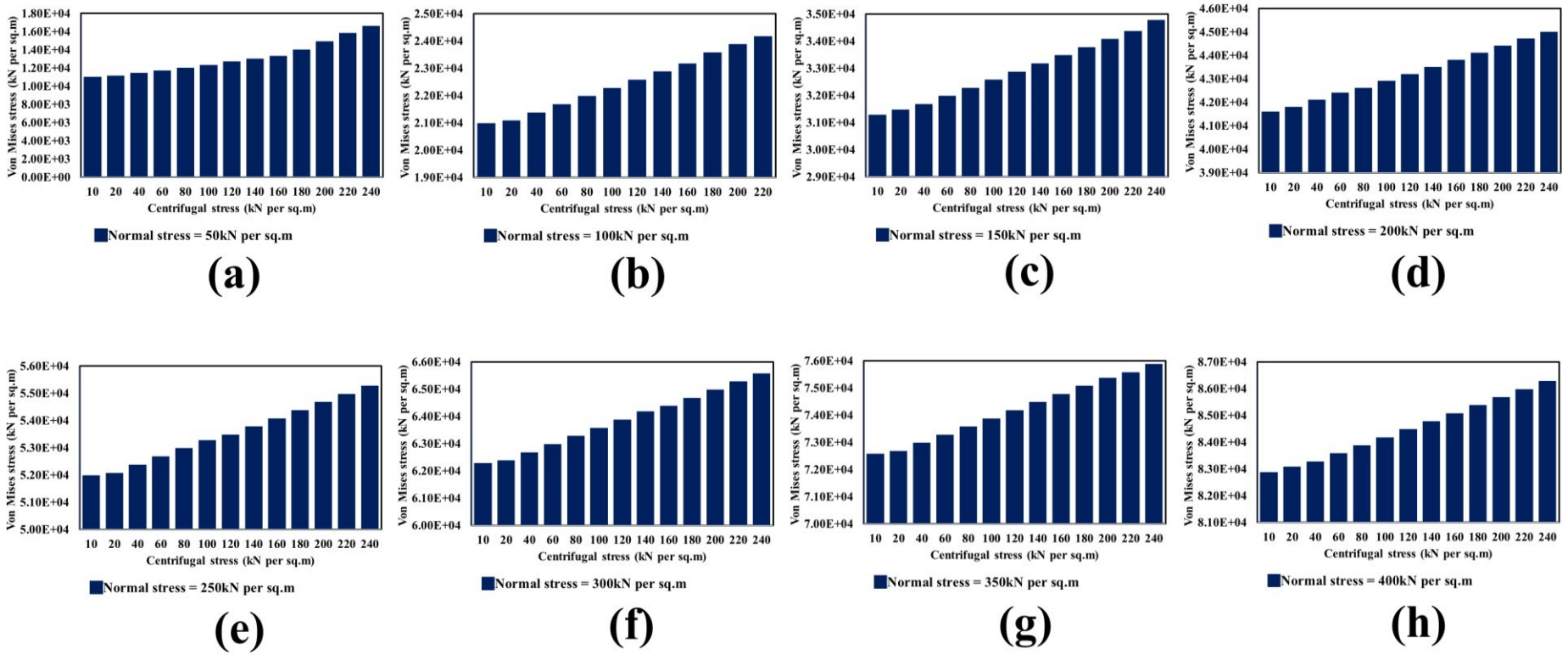

Figure 10. Variation of maximum Von Mises stress ($\boldsymbol{kN/m^2}$) against centrifugal stress ($\boldsymbol{kN/m^2}$) - $\boldsymbol{t = 7mm}$

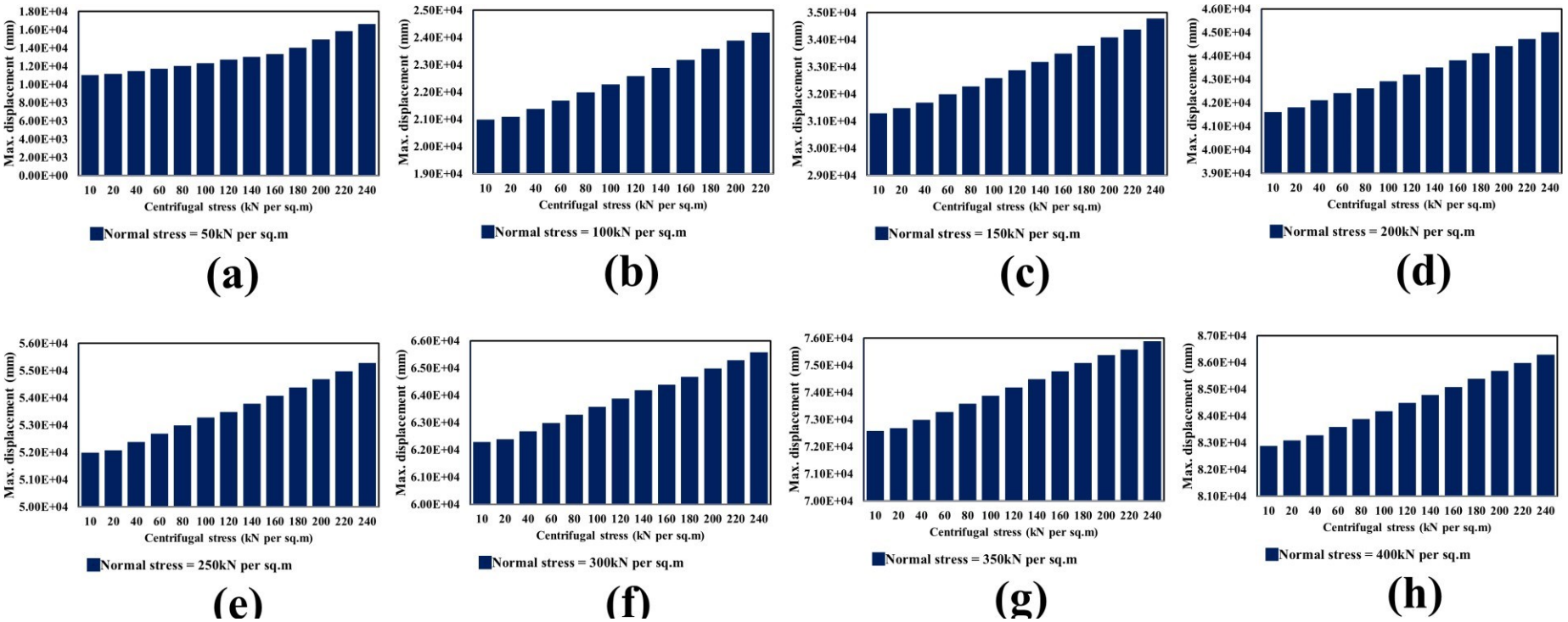

Figure 11. Variation of maximum displacement ($\boldsymbol{mm}$) against centrifugal stress ($\boldsymbol{kN/m^2}$) - $\boldsymbol{t = 9mm}$

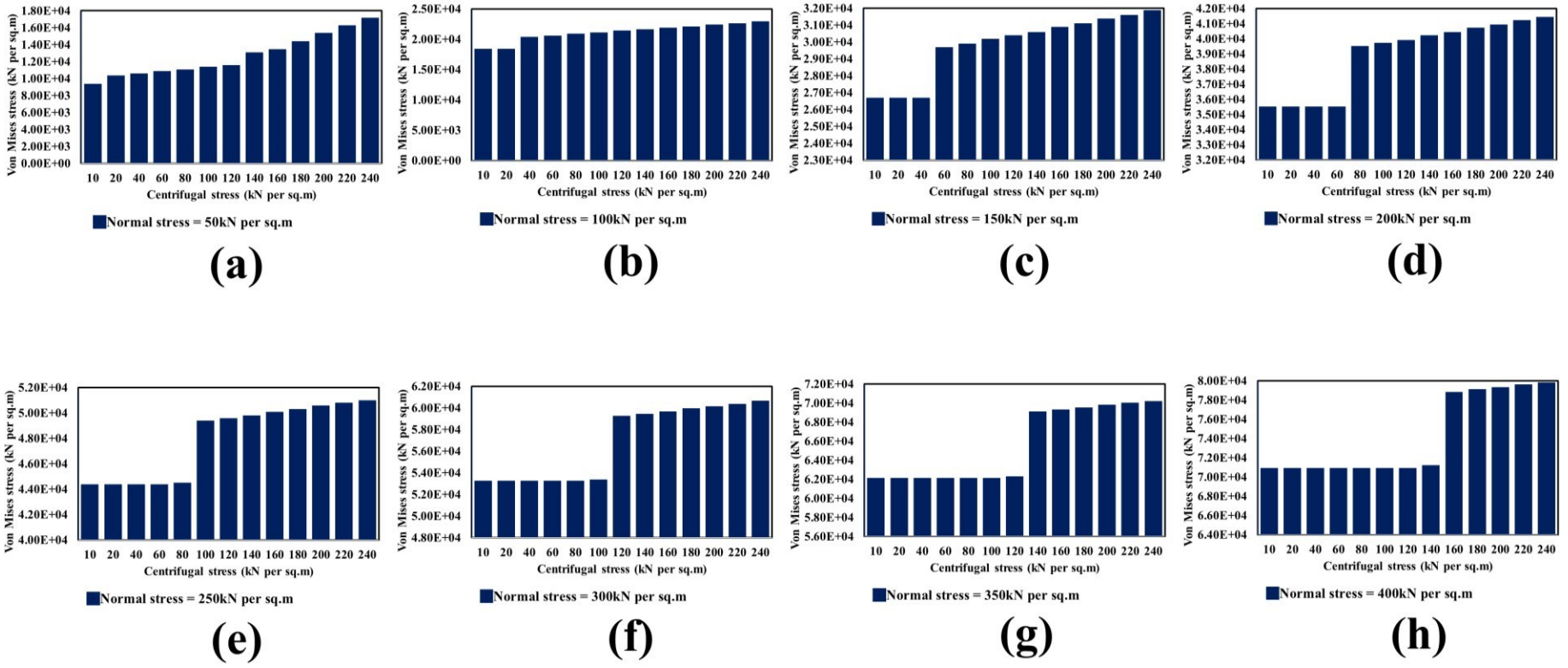

Figure 12. Variation of maximum Von Mises stress ($\boldsymbol{kN/m^2}$) against centrifugal stress ($\boldsymbol{kN/m^2}$) - $\boldsymbol{t = 9mm}$

In an FEA case study, as depicted in Figure 6-Figure 12, results show that the maximum displacement of the Alumadeck^{TM} increases linearly with an increase in the centrifugal stresses signifying a positive correlation. The maximum Von Mises stresses are within acceptable limits since they are less than the factored yield stress of the deck, and this is a measure of the durability of the Alumadeck^{TM}. The maximum displacements obtained for the $5mm$, $7mm$ and $9mm$ stiffner thicknesses are $0.004mm$, $0.0033mm$ and $0.003mm$ respectively, which is found to be less than the allowable displacement prescribed in design standards for all plates. Based on these results, it is recommended that the thickness of stiffners should be a minimum of $t_{stiffner} = 7mm$ to have a durable structure since some of the maximum displacements for lower dimensions and Von Mises criteria, with reference to Subsection 3.1.2 such as for $t_{stiffner} = 5mm$ were not satisfactory. Hence, the displacements are acceptable for the selected geometric dimensions employed for the SRA later in the upcoming Subsection 4.2, indicating the durability of the Alumadeck^{TM} with these properties.

Furthermore, this case study revealed that the measured stiffner thickness assumed to suffice to satisfy safety and durability criteria can optimise the deck structure in terms of reducing the structure's self-weight saving manufacturing cost of more than 25% when compared with values suggested in Refs. (Formisano et al. 2016; Mazzolani 2006; Siwowski 2006a, 2009a; b).

4.1.2 Validation

In order to validate the structural FEA model developed, the results of the deformation analysis at salient points on the structure was compared against results from structural mechanics equations (coded in MATLAB), Equation (19)-(31) summarised in Subsection 3.4 for the same test structural configuration set-up. Results of the assessment show that there is good agreement in the deflection calculated using the analytical method compared to the developed FEA model approximately predicts (since the percentage difference calculated is less than ten (10%)), which demonstrates the scientific soundness of the FEA model adopted herein. Response surface modelling (RSM) methodologies are now extensively used within the field of SRA, as noted by several studies (Al-Sanad et al. 2021; Ivanhoe et al. 2020; Kolios et al. 2018; Shittu 2020; Shittu et al. 2020d, c; a, 2021) owing to their capability of enhanced LSF approximations with high fidelity. LSF concepts as derived from these sources are adapted in the present study as presented in the upcoming Subsections.

4.2 Stochastic assessment

The SRA of the aluminium alloy deck system is evaluated for the Alumadeck^{TM}–steel girder section considering the system I and II, applying the validated model in Subsection 4.1.2. The composite is designed per the AASHTO guidelines (AASHTO 2007). The girder examined in the present study is assumed to be simply supported. The horizontally curved steel I-girder bridge considered is assumed as a single span with four girders in the cross-section. Figure 13 illustrates a schematic depicting the configuration of the girders stiffened and the cross frames.

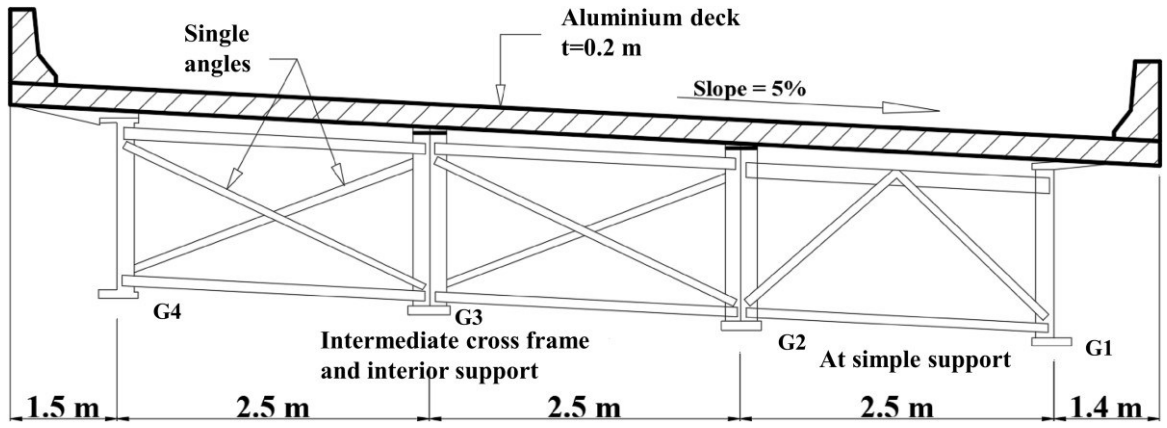

Figure 13. I-girder bridge cross-section showing the cross frames. Source: Ref. (J.M. et al. 2005).

4.2.1 Radial moment and shear force acting on deck

Using the curved deck with reference to Subsection 2.3.1: Figure 2, and Equations (1)-(24) are solved simultaneously to obtain the radial moment and shear force by applying boundary conditions. It is assumed that the panel span considered is the spacing between two girders. Where the following conditions apply: (1) $\eta = 0$, at $r = r_0 = 93.6m$ thus $X = \frac{r_0}{r} = 0.936$ (2) $\eta = 0$, at $r = r_i = 91.1m$ thus $X = \frac{r_i}{r} = 0.911$ (3) $M_r = 0$, at $r = r_i = 92.35m$, thus $X = \frac{r_i}{r} = 0.9235$ (4) $M_r = 0$, at $r = r_0 = 89.7m$, thus $X = \frac{r_0}{r} = 0.897$. The unknowns $A, B, C\ and\ D$ can be determined after which M_r and R_r are obtained for the HL93 loading condition.

4.2.2 Bridge deck design parameters and design data for I-girder G4

As derived from Ref. (Heins 1975), the minimum radius for the design of a horizontally curved bridge is $100m$. The following parametric values defined in Table 1 below were assumed for the curved deck with reference to Figure 2 and used in the design.

Table 1. Parameters of interest in the design model

Parameter	Value
Radius	$100m$
Bridge span	$20m$
Deck thickness, h	$200mm$
D_r	$5.2071 \times 10^9 Nm^2$
D_θ	$5.2071 \times 10^9\ Nm^2$
H	$5.1029 \times 10^9\ Nm^2$
m_1	1.633687
m_2	0.366313
m_3	2.36496
m_4	0.36496
$M_{radial}(kNm)$ for ULS	140
$R_{radial}(kN)$	0.142
Aluminium alloy deck compressive strength, F_c	$170MPa$
Yield strength, F_y	$170MPa$
Ultimate strength, F_u	$205MPa$
Effective area of the aluminium alloy deck/ slab (long term), A_{s_3n}	60,090.202 mm^2
Short term effective area of deck, A_{s_n}	180,270.606 mm^2
Structural steel	ASTM A709 grade 50W (yield strength, $F_y = 350MPa$)
Live load	HL93 (AASHTO 2007)
Unit weight of deck	26.9 kN/m^3
Unit weight of steel	78.5 kN/m^3
Future wearing surface	6.73 kN/m^3
Elastic modulus of aluminium, E_{AL}	69.6 GPa
Elastic modulus of steel, E_{ST}	200 GPa
Girder depth, d	2.4 m
Web thickness, t_w	1.6 cm
Flange thickness; top (compression flange) and bottom (tension flange), t_{fc} and t_{ft}	2.1 cm
Flange width, b_f	50 cm

The composite (i.e. the deck and I-girder) is designed against the strength LS. Also, the outermost girder (G4), which is the most critical, is analysed. Ref. (Eurocode 9 1999) stipulates that the tensile yield strengths should be multiplied by 0.8. According to AASHTO (AASHTO 2010), the dead load includes the weight of all structure components, appurtenances and utility, earth cover, future overlay, and planned widening. The dead load is subdivided into three categories: (1) Dead load of a structural component (DC): This is divided into DC1 and DC2. DC1 accounts for the weight of the deck and the steel, while DC2 accounts for the dead weight of the parapets. For the Aluminium alloy deck: $DC1 = 26.9 \times 0.2 = 5.38\ kN/m$, while for the steel girder: $DC1 = 78.5 \times 0.021 = 1.65\ kN/m$. (2) Dead load wearing course (DW): This accounts for the future wearing course. Thus, $DW = 6.73 \times 0.0095 = 0.064 kN/m$.

The AASHTO vehicular live load is designated as HL-93 loading and is a combination of a design truck or a tandem plus the design lane load. The design truck specified comprises a $36kN$ lead axle spaced $4.287m$ from the closer of the two $144kN$ rear axle, which has variable spacing from 4.287 to $9.144m$. The transverse spacing is $1.83m$. The design truck occupies $3.045m$ lane width, is positioned within the design lane to produce maximum force effect, and must not be closer than $0.61m$ from the face of the edge of the design lane.

4.2.3 Design moment

In this study, the position that yields the maximum stress in the deck for single-lane and two-lane loaded bridges is adopted (i.e. HL-93 loading). See Figure 2. For a straight girder, the maximum moment can be expressed as $M = \frac{wl^2}{8}$ and $S = \frac{M4}{l}$ where $M =$ Maximum moment in the girder, $w =$uniformly distributed load along the length of the girder, l= the girder span length. For the horizontally curved aluminium alloy deck and Steel girder: $M_{radial\ DC1} = 140kNm$ (i.e. for Aluminium); $M_{radial\ DC1} = KM_{DC1} = 1.0 \times 1.65 \times \frac{20^2}{8} = 82.5kNm$, for the Steel girder (See Equation (24)). For the parapet: $M_{radial\ DC2} = KM_{DC2} = 1.0 \times 6.32 \times 0.5 \times \frac{20^2}{8} = 158kNm$. For the polymer surface, $M_{radial\ DW} = \frac{KM_{DW}}{4} = \frac{1.0}{4} \times 0.064 \times 2.18 \times \frac{20^2}{8} = 1.744\ kNm$.

The live load component for the SRA was determined using a design truck co-occurring with a uniformly distributed lane load. The maximum moment occurs when the first rear axle is $0.055m$ from the centre of the girder span as the truck moves eastwards on the bridge. Live load is due to three lanes of LRFD HL-93 plus appropriate centrifugal force effects. The DLA has been applied to live load. The overturning impact of the centrifugal force has been considered by increasing the exterior wheel load and decreasing the interior wheel load in each lane. The live load was also multiplied by 0.85 in the analysis to account for the probability of multiple presences.

$$R_1 + R_2 = 324kN \quad (32)$$

$$-20R_1 + 144(12.57) + 144(9.945) + 36 \times 6.825 = 0 \quad (33)$$

$$R_1 = \frac{1}{20}(3487.86) = 174.39kN \quad (34)$$

$$R_2 = 149.607kN \quad (35)$$

$$M_{max} = 10R_1 - 144(3.061) = 1{,}302.57kNm \quad (36)$$

$$M_{\mathrm{HL93\ LL+IM}} = 1472.56kNm \quad (37)$$

4.3 Bridge component design and derivation of LSFs

In this study, a detailed calculation for girder flexural design based on the AASHTO (AASHTO 2007). The design is carried out for the critical section for girder G4 for the strength LS under the strength-I load combination on the completed structure. Further advanced design and stochastic optimisation calculations concerning this as carried out by the same author can be found in Ref. (Shittu 2015).

4.3.1 Girder stress check the critical section on G4 – section proportioning

For a web without longitudinal stiffners, the web is proportioned such that: $\frac{D}{t_w} \leq 150$; $\frac{2.358}{0.016} = 147.38 < 150$ **OK.** Compression and tension flange are proportioned such that: $\frac{b_f}{2t_f} \leq 12$; $\frac{50}{2(2.1)} = 11.9$ – Thus, both Flanges **OK.** $b_f \geq \frac{D}{6}$; $\frac{2.358}{6} = 0.393\ m = 39.3\ cm$ – Thus, both Flanges **OK** $t_f \geq 1.1t_w$; $1.1(1.6) = 1.76\ cm$, Both Flanges **OK.** $0.1 \leq \frac{I_{yc}}{I_{yt}} \leq 10$; $I_{yc} = I_{yt} = 2.1 \times \frac{(50)^3}{12} = 21875 cm^4$; $\frac{I_{yc}}{I_{yt}} = 1$ – **OK.** Therefore, from the foregoing, it can be inferred that all section proportions for this location are satisfied.

4.3.2 Girder stress check critical section (mid-span) on G4 transversely stiffened web – strength – top flange

The factored vertical bending stress in the top flange due to dead and live load, f_{bu} is given as (J.M. et al. 2005):

$$f_{bu,c} = [\frac{1.25M_{DC1}C_{nc}}{I_{nc}} + \frac{(1.25M_{DC2} + 1.5M_{DW})C_{3n}}{I_{3n}} + \frac{1.75M_{LL}C_n}{I_n}] 12\eta \quad (38)$$

But, $\eta = 1$, where C_{3n} is the centroid considering long term composite properties, C_n is the centroid considering short term, C_{nc} is the centroid considering non-composite, I_{nc} is the moment of inertia for the non-composite section. For long term composite section properties (3n), effective width of slab,

$$b_{s\_3n} = \frac{b_{slab}}{3n} \quad (39)$$

While for the short term (n),

$$b_{s\_n} = \frac{b_{slab}}{n} \quad (40)$$

The neutral axis for the non-composite action, C_{nc}

$$D_c = \frac{A_{fc}(\frac{t_{fc}}{2}) + A_{ft}(D - \frac{t_{ft}}{2})\ A_{web}(\frac{D}{2} + t_{fc})}{A_{girder}} - t_{fc} \quad (41)$$

The neutral axis for the composite action, $C_{n/3n}$

$$NA = \frac{A_{fc}(t_s + t_{haunch} - \frac{t_{fc}}{2}) + A_{ft}(D + t_s + t_{haunch} + \frac{t_{ft}}{2}) + A_{web}(\frac{D}{2} + t_s + t_{haunch}) + A_s\frac{t_s}{2}}{A_{Total}} \quad (42)$$

A_{fc} is the area of compression flange, A_{ft} is the area of the tension flange, t_s is the thickness of slab, t_{haunch} is the thickness of the haunch, D is the depth of the web, t_{fc} is the thickness of compression flange, A_w is the area of web, t_w is the thickness of web and b_{fc} is the width of the compression flange. The neutral axis is measured from the top of the deck. The moment of inertia considering non-composite action is given by:

$$I_{nc} = \frac{b_{fc}t_{fc}^3}{12} + [A_{fc}\,(D_c + t_{fc} - \frac{t_{fc}}{2})^2] + \frac{b_{ft}t_{ft}^3}{12} + [A_{ft}\,(d - (D_c + t_{fc}) - \frac{t_{ft}}{2})^2] + \frac{t_w D^3}{12} + A_w\,(D_c + t_{fc} - t_{fc} - \frac{D}{2})^2. \quad (43)$$

The moment of inertia considering composite action, (i.e. short/long term) is expressed as:

$$I_{n/3n} = \frac{b_{fc}t_{fc}^3}{12} + [A_{fc}\,(NA - t_s - t_{haunch} + \frac{t_{fc}}{2})^2] + \frac{b_{ft}t_{ft}^3}{12} + [A_{ft}\,(t_s + t_{haunch} + D + t_{ft} - NA - \frac{t_{ft}}{2})^2] + \frac{t_w D^3}{12} + A_w\,(NA - t_s - t_{haunch} - \frac{D}{2})^2 + \frac{b_s t_s^3}{12} + A_s\,(NA - \frac{t_s}{2})^2. \quad (44)$$

The compression flange must satisfy the following relation:

$$f_{bu} \leq \phi_f F_{nc} \quad (45)$$

ϕ_f is the resistance factor (RF), where:

$$F_{nc} = R_b R_h F_{yc} \quad (46)$$

R_b is the web load shedding factor = 1, for $\frac{D}{t_w} < 150$, R_h is the hybrid factor = 1 and F_{yc} represents the yield strength for the compression flange. The LSF for the top flange of a transversely stiffened web (i.e. the strength LSS) can be expressed as:

$$G(x) = \phi_f F_{yc} - f_{bu} = \phi_f F_{yc} - [\frac{1.25M_{DC1}C_{nc}}{I_{nc}} + \frac{(1.25M_{DC2} + 1.5M_{DW})C_{3n}}{I_{3n}} + \frac{1.75M_{LL}C_n}{I_n}]\,12\eta \quad (47)$$

The ductility requirements have to be checked to prevent the aluminium deck from premature crushing.

$$D_p \leq 0.42D_t \quad (48)$$

where D_t is the total depth of the composite section expressed as:

$$D_t = D + t_{haunch} + t_{slab} + t_{ft} \quad (49)$$

D_p is the distance from the top of the deck to the neutral axis of the composite section at the plastic moment:

$$D_p = Y_{bar} + t_{slab} + t_{haunch} \quad (50)$$

$P_s = f_s A_s = 205 \times 60090.202 \times 10^{-3} = 12318.5kN$ - Force in the slab; $P_c = f_{yc}A_{fc} = 350 \times 500 \times 21 \times 10^{-3} = 3675kN$ - Force in the compression flange; $P_t = f_{yt}A_{ft} = 3675kN$ - Force in the tension flange; $P_w = f_{yw}A_w = 350 \times 16 \times 2358 \times 10^{-3} = 13204.8kN$ - Force in the web. If $P_t + P_w \geq P_c + P_s$, then the plastic neutral axis is in the web: $16879.8 > 15993.5$. Therefore, the PNA is on the web and $\bar{Y}$ or

$$Y_{bar} = \frac{D}{2}\left(\frac{P_t - P_c - P_s}{P_w} + 1\right) \quad (51)$$

4.3.3 Girder Stress Check Strength Limit State - Web

According to the AASHTO specifications, composite sections subjected to positive flexure, as in this case study, need not be checked for web bend-buckling in its final composite condition when the web does not require longitudinal stiffners.

4.3.4 Girder stress check critical section (at mid-span) on G4 transversely stiffened web – strength – bottom flange

The tension flange must satisfy the following relation:

$$f_{bu} + \frac{1}{3} f_l \leq \phi_f F_{nt}. \quad (52)$$

The factored bottom flange vertical bending stress due to dead and live load is expressed as:

$$f_{bu,T} = \left[\frac{1.25M_{DC1}C_{nc}}{I_{nc}} + \frac{(1.25M_{DC2}+1.5M_{DW})C_{3n}}{I_{3n}} + \frac{1.75M_{LL}C_n}{I_n}\right]12\eta. \quad (53)$$

The lateral bending stress at the cross-frame due to curvature, f_l is given as (AASHTO 2007):

$$M_{lat\_NC} = \lambda M_{DC1} \quad f_{l\_NC} = \frac{M_{lat\ NC}}{S_{bot\_fl}} \quad (54)$$

$$M_{lat\_C1} = \lambda M_{DC2} \quad f_{l\_C1} = \frac{M_{lat\ C1}}{S_{bot\_fl}} \quad (55)$$

$$M_{lat\_C2} = \lambda M_{Dw} \quad f_{l\_C2} = \frac{M_{lat\ C2}}{S_{bot\_fl}} \quad (56)$$

$$M_{lat\_LL} = \lambda M_{LL} f_{l\_LL} = \frac{M_{lat\ LL}}{S_{bot\ fl}} \quad (57)$$

λ is as specified in Ref. (J.M. et al. 2005), the total factored lateral bending stress:

$$f_l = 1.25(f_{l\_NC} + f_{l\_C1}) + 1.5(f_{l\_C2}) + 1.75(f_{l\_LL}). \quad (58)$$

The nominal flexural resistance, $M_n = M_p$ if $D_p \leq 0.1D_t$; otherwise,

$$M_n = M_p\left(1.07 - \frac{0.7D_p}{D}\right)_t. \quad (59)$$

Yield moment associated with the strength-I limit state (AASHTO 2007)

$$M_{D1t} = f_{D1t}S_t,\ M_{D1c} = f_{D1c}S_c,\ M_{D2} = M_{DC2} + M_{DW} \quad (60)$$

Tension flange

$$M_{ADt} = \left(f_{yt} - \frac{M_{D1t}}{S_t} - \frac{M_{D2}}{S_{t3n}}\right)S_{tn} \quad (61)$$

$$M_{yt} = M_{D1t} + M_{D2} + M_{ADt} \quad (62)$$

Compression flange

$$M_{ADc} = \left(f_{yc} - \frac{M_{D1c}}{S_c} - \frac{M_{D2}}{S_{c3n}}\right)S_{cn} \quad (63)$$

$$M_{yc} = M_{D1c} + M_{D2} + M_{ADc} \quad (64)$$

Section modulus,

$$S_{xt} = \frac{M_{yt}}{f_{yt}} \quad (65)$$

Strength limit check is **OK** if

$$M_u + \frac{f_l \mathcal{S}_{xt}}{3} \leq \phi M_{fn} \tag{66}$$

$$M_u = 1.25M_{uDC2} + 1.5M_{uDW} + 1.75M_{uLL} \tag{67}$$

The LSF for strength criteria can be expressed as

$$G(x) = \phi_f M_n - M_u - \frac{f_l \mathcal{S}_{xt}}{3} \tag{68}$$

or,

$$G(x) = \phi_f f_{nt} - f_{bu} - \frac{f_l}{3} \tag{69}$$

4.3.5 Girder stress check critical section (at mid-span) on G4: transversely stiffened web – shear strength – web

The shear strength of the mid-span in girder G4 is determined as:

$$V_u \leq \phi_v V_n \tag{70}$$

where: V_u=shear in the web at the section under consideration due to factored loads; V_n=nominal shear resistance; ϕ_v = RF for shear taken as 1.0.

$$V_n = CV_p \tag{71}$$

$$V_p = 0.58F_y D t_w \tag{72}$$

where C is the ratio of the shear-buckling resistance to the shear yield strength

$$\frac{D}{t_w} > 1.40\sqrt{\frac{Ek}{F_{yw}}} \tag{73}$$

where k is the shear buckling coefficient $= 5 + \frac{5}{\left(\frac{do}{D}\right)^2} = 10$

$$147.4 > 1.4\sqrt{\frac{200000(10)}{350}} = 75.6. \tag{74}$$

Therefore $C = \frac{1.57}{\left(\frac{D}{t_w}\right)^2}\left(\frac{Ek}{F_{yw}}\right)$

$$G(x) = \phi_v V_n - V_u \tag{75}$$

Having completed the critical design exercise as elucidated above, Subsection 4.3, we now proceed into the stochastic optimisation by deriving the LSF - Equations (**38**)-(**75**) and then perform the FORM simulation executed in MATLAB (entirely implemented by the same authors (Shittu 2020; Shittu et al. 2020b, d, c; a, 2021)) applying the stochastic variables defined in Table 2 to calculate the reliability indices. The HL-RF recursive FORM algorithm developed by the same authors in Refs. (Shittu 2020; Shittu et al. 2020b, d, c; a, 2021) are adapted for the present study. The iterative FORM algorithm has been validated against the MCS in previous studies (Shittu et al. 2020d; c). The well-established FORM is used as it offers a good balance between efficiency and accuracy for realistic problems. One limitation of the MCS method is that many simulations are required (i.e. requiring an excessive computational effort) to calculate the very low values of failure probability, which is a characteristic of complex offshore structures (Shittu et al. 2020d, 2021). The FEA and SRA results of this study considering the strength LS is depicted in see Figure 6-Figure 14:

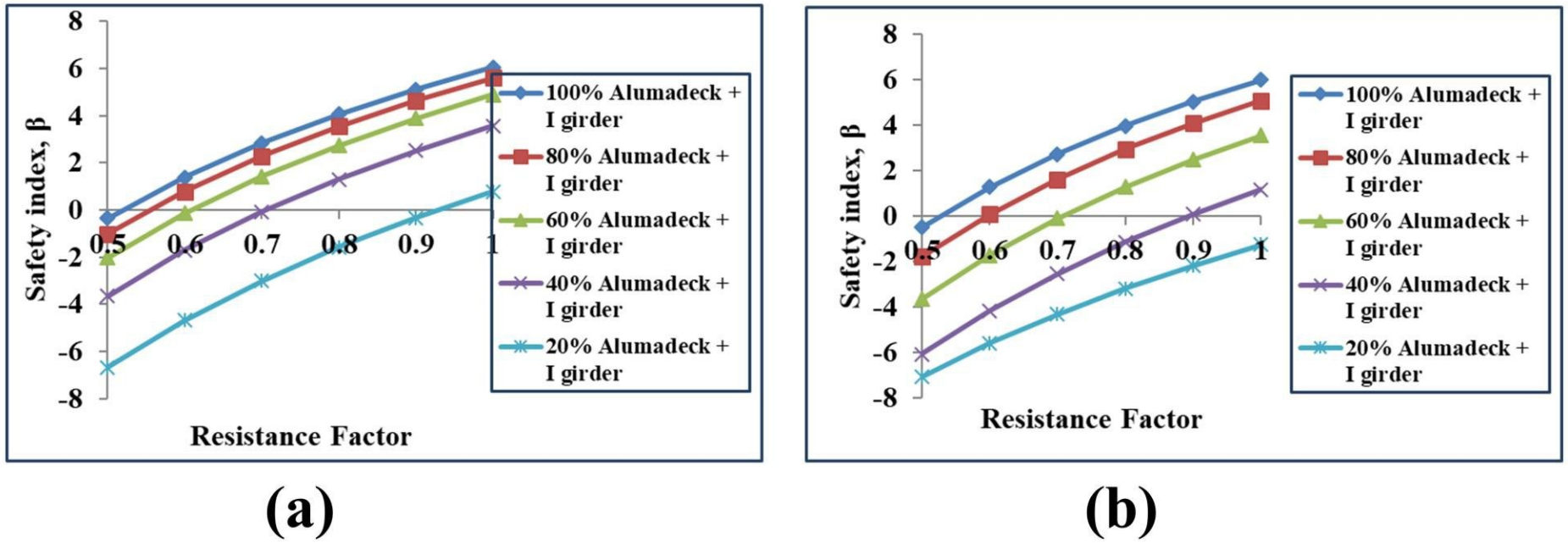

Figure 14. RI at various RFs at varying Alumadeck^{TM}-I-girder composite action: (a) Considering the failure of the top flange, (b) Bottom flange.

Table 2. Parameters of the stochastic model for the strength limit state (Ellingwood et al. 2014; Ren et al. 2021; Wang et al. 2016a, 2011b; a; Wang and Ellingwood 2015; Yanweerasak et al. 2018)

Var. no.	Variable	Meaning	Distribution type	Expected value E_x	Coefficient of variation	Standard deviation
X1	M_{DC1}	Moment due to curved aluminium deck and steel girder	Log-Normal	$222.5kNm$	0.12	$26.7kNm$
X2	M_{DC2}	Moment due to parapet	Log-Normal	$158kNm$	0.12	$18.96kNm$
X3	M_{DW}	Moment due to polymer surface	Log-Normal	$1.7\ 44kN$	0.12	$0.209kNm$
X4	M_{LL}	Moment due to live load	Log-Normal	$1473kNm$	0.12	$176.76kNm$
X5	t_f	Thickness of flange	Normal	$0.021m$	0.03	$6.3 \times 10^{-4}m$
X6	b_f	Flange width	Normal	$0.5m$	0.03	$0.015m$
X7	d	Depth of section	Normal	$2.4m$	0.03	$0.072m$
X8	t_w	Thickness of web	Normal	$0.016m$	0.03	$4.8 \times 10^{-4}m$
X9	D	Distance from bottom of top flange to top of bottom flange	Normal	$2.358m$	0.03	$0.07074m$
X10	t_{slab}	Slab thickness	Normal	$0.2m$	0.03	$6 \times 10^{-3}m$
X11	t_{haunch}	Haunch thickness	Normal	$0.09m$	0.03	$2.7 \times 10^{-3}m$
X12	A_{slab_3n}	Long term Area of slab	Normal	$0.06m^2$	0.03	$1.8 \times 10^{-3}m^2$
X13	A_{slab_n}	Area of slab short term	Normal	$0.18m^2$	0.03	$5.4 \times 10^{-3}m^2$
X14	ϕ_f	Resistance factor (RF)	Normal	1	0.05	0.05
X15		Percentage composite action	Normal	100%	0.02	2%
X16	f_y	Yield stress	Log-Normal	$3.5 \times 10^5 kN/m^2$	0.02	$7 \times 10^3 kN/m^2$

4.3.6 Stochastic optimisation

This Subsection presents the results of the optimisation exercise, Figure 6- Figure 14: On completion of the probabilistic assessment, the result recorded that the RI is sensitive to the RF, and the RI also increases linearly with an increase in RF, signifying a positive correlation. Also, the results reveal that the design is not acceptable for an RF of 0.5 at 100% and 80% composite action in both compression and tension flanges. The design is also unacceptable for an RF of 0.6 and below at 60% composite action for both flanges; 0.7 and below at 40% and completely unacceptable at 20% composite action. For 80% composite action at an RF of 0.8, the safety index is 3.55, considering the failure of the compression flange. The tension flange is 3.0, which is ideal to guarantee the structure's safety. This

shows that an I Girder of a depth of $2.4m$, flange thicknesses of $21mm$, flange width of $500mm$ and web thickness of $16mm$ is safe to carry the truck loads.

The SRA framework developed herein will be an invaluable tool for designers with respect to reliability-based design optimisation. Bridge industry practitioners can harness the framework's capability to address the problem of optimising the manufacturing expenditure, which is an issue of priority and hence allows cost reduction activities needed to ensure structural safety and efficient performance of the bridge structures.

5 Conclusion and future insights

5.1 Conclusion

In this study, the FE and SRA of a horizontally curved aluminium alloy bridge deck on steel I-girders is presented. For the purpose of calculating the critical response of the structural assembly, an FEA model was developed in the ABAQUS© environment (a well-established FEA modelling software, thanks to its high fidelity and precision). A probabilistic analysis was conducted using the FORM coded in MATLAB to predict the RI (β) at various percentages of composite actions while varying geometric dimensions. From the results revealed herein, the following conclusions could be inferred:

- A novel FEA model of a horizontally curved Alumadeck^{TM} was developed to calculate the critical responses of the structure in the presence of truck HL-93 loading configuration.
- In a case study, it was revealed from FEA response results that the thickness of stiffners, $t_{stiffner}$ should be a minimum of 7mm to have a safer structure since some of the maximum displacements for the 5mm were not satisfactory, which could result in savings of more than 25% in production costs compared with what is obtained in the existing design
- These critical responses predicted using the FEA is entered into the LSF subroutine (derived via AASHTO LRFD flexural resistance formulation) of the stochastic model in an HL-RF iterative FORM algorithm executed in the MATLAB environment
- It is shown that the propriety Alumadeck^{TM} system conforms with the Load Resistance Factor Design (LRFD) Specification, which stipulates that the target value of reliability index as 3.5 for a resistance factor of 1.0 (assuming 80% composite action compression flange).
- The result of the composite action between the deck and the girder for RF of 1.0 for full composite action (i.e. considering the failure of the bottom flange) shows a safety index within the acceptable limit which shows that the Alumadeck^{TM} can withstand the live load it is subjected to considering the HL-93 loading condition. Also, it can be established that from this study that the RI is sensitive to the RF.

5.2 Future insights

Research into the structural application of aluminium alloys in civil engineering structures is disappointingly sparse. Most future developments are likely to arise from advances in other applications, such as the aerospace and transport industries, with different criteria to address. Traditionally, castings have been discouraged for structural applications, as many castings' quality and brittle characteristics have been unsuitable. The automotive and aerospace industries have developed the use of high-precision castings that have good ductility and are increasingly using these in combination with purpose-designed extrusions. Such methods are particularly appropriate for volume production. The technology is likely to be useful in civil engineering if sufficient quantities can justify developing and tooling costs for any specific project or proprietary system. Development of material technology continues. New processes using fibre-reinforced aluminium and powder metallurgy promise stronger and stiffer alloys than the current alloys in structural use. The increase in stiffness will be particularly relevant. Technology for joining materials is an area of research and development that transcends different industries quite well. Results in friction stir welding and adhesive bonding over the past ten years have yet to become firmly established in the civil engineering industry. They are not

covered in detail by the current design codes. They are, however, well established in the manufacture of railway carriages and military bridging.

6 References

A.O., A., O.S., A., and A.T., O. (2010). "Probabilistic Evaluation of Aluminum Bridge Decks Design Criteria on Steel Girders." *Journal of Engineering and Applied Sciences*, 5(1), 4–13.

AASHTO. (2007). "Guide Specifications for Horizontally Curved Steel Girder Highway Bridges with Design Examples for I-Girder and Box-Girder Bridges", „." American Association of State and Highway Transportation Officials, Washington D.C., USA.

AASHTO. (2010). "LRFD Bridge Design Specifications." American Association of State Highway and Transportation Officials, Washington, DC, USA.

Achmus, M., and Abdel-Rahman, K. (2005). "Finite element modelling of horizontally loaded monopile foundations for offshore wind energy converters in Germany." *Frontiers in Offshore Geotechnics*,(August 2005).

Al-Sanad, S., Wang, L., Parol, J., and Kolios, A. (2021). "Reliability-based design optimisation framework for wind turbine towers." *Renewable Energy*, Elsevier Ltd, 167, 942–953.

Beck, A. T., and Gomes, W. J. D. S. (2012). "A comparison of deterministic, reliability-based and risk-based structural optimization under uncertainty." *Probabilistic Engineering Mechanics*, Elsevier, 18–29.

Breitung, K. (2015). "40 years FORM: Some new aspects?" *Probabilistic Engineering Mechanics*, 42, 71–77.

BS5400-2. (1978). "BSI Steel, Concrete and Composite Bridges." British Standard Institution, London, UK.

Choi, S.-K., Grandhi, R., and Canfield, R. (2006). *Reliability-based Structural Design*. Springer, USA.

Ditlevsen, O., and Madsen, H. O. (2007). *Structural Reliability Methods*. Wiley New York.

Ellingwood, B. R. (2005). "Risk-informed condition assessment of civil infrastructure: state of practice and research issues." *Structure and Infrastructure Engineering*, 1(1), 7–18.

Ellingwood, B. R., Vrouwenvelder, T., and Gulvanessian, H. (2014). "Eurocodes and their implications for bridge design: Background, implementation, and comparison to North American practice." *Journal of Bridge Engineering*, 19(1), 3–4.

Eurocode 9. (1999). "Design of Aluminium Structures." Centroum Hout, the Netherlands.

Formisano, A., De Matteis, G., and Mazzolani, F. M. (2016). "Experimental and numerical researches on aluminium alloy systems for structural applications in civil engineering fields." *Key Engineering Materials*, Trans Tech Publications Ltd, 256–261.

Gentils, T., Wang, L., and Kolios, A. (2017). "Integrated structural optimisation of offshore wind turbine support structures based on finite element analysis and genetic algorithm." *Applied Energy*, Elsevier Ltd, 199, 187–204.

Ghosn, M., Frangopol, D. M., McAllister, T. P., Shah, M., Diniz, S. M. C., Ellingwood, B. R., Manuel, L., Biondini, F., Catbas, N., Strauss, A., and Zhao, X. L. (2016). "Reliability-based performance indicators for structural members." *Journal of Structural Engineering (United States)*, 142(9), 1–13.

Guo, T., Sause, R., Frangopol, D. M., and Li, A. (2011). "Time-dependent reliability of PSC box-girder bridge considering creep, shrinkage, and corrosion." *Journal of Bridge Engineering*, 16(1), 29–43.

Heins, C. P. (1975). *Bending and Torsional Design in Structural Members*. Lenington Books, DC Health Company, London, UK.

Heins, C. P., and Hails, R. L. (1969). "Behaviour of Stiffened Curved Plate Model." *ASCE Structural Division,S T11*, 95, 2353–2369.

Imam, B. M., Chryssanthopoulos, M. K., and Frangopol, D. M. (2012). "Fatigue system reliability analysis of riveted railway bridge connections." *Structure and Infrastructure Engineering*, 8(10), 967–984.

Ivanhoe, R. O., Wang, L., and Kolios, A. (2020). "Generic framework for reliability assessment of offshore wind turbine jacket support structures under stochastic and time dependent variables." *Ocean Engineering*, Elsevier Ltd, 216, 107691.

J.M., K., W.G., W., C., S., and K., J. (2005). *AASHTO-LRFD Design Example Horizontally Curved Steel I-Girder Bridge, .* USA.

Kolios, A., Di Maio, L. F., Wang, L., Cui, L., and Sheng, Q. (2018). "Reliability assessment of point-absorber wave energy converters." *Ocean Engineering*, Elsevier Ltd, 163(October 2017), 40–50.

Kolios, A., and Wang, L. (2018). "Advanced reliability assessment of offshore wind turbine monopiles by combining reliability analysis method and SHM / CM technology." 1412–1419.

Kwon, K., and Frangopol, D. M. (2011). "Bridge fatigue assessment and management using reliability-based crack growth and probability of detection models." *Probabilistic Engineering Mechanics*, Elsevier Ltd, 26(3), 471–480.

Li, H., Frangopol, D. M., Soliman, M., and Xia, H. (2016). "Fatigue Reliability Assessment of Railway Bridges Based on Probabilistic Dynamic Analysis of a Coupled Train-Bridge System." *Journal of Structural Engineering (United States)*, 142(3), 1–16.

Linzell, D., Chen, A., Sharafbayani, M., Seo, J., Nevling, D., and Ashour, O. (2010). *Guidelines for Analyzing Curved and Skewed Bridges and Designing theem for Construction*. USA.

Mazzolani, F. M. (2006). "Structural applications of aluminium in civil engineering." *Structural Engineering International: Journal of the International Association for Bridge and Structural Engineering (IABSE)*, Int. Assoc. for Bridge and Structural Eng. Eth-Honggerberg, 16(4), 280–285.

Melchers, R., and Andre, T. (2018). *Structural reliability analysis and prediction*. Wiley, Hoboken, USA.

Nie, J., and Ellingwood, B. R. (2005). "Finite element-based structural reliability assessment using efficient directional simulation." *Journal of Engineering Mechanics*, 131(3), 259–267.

Nowak, A. S. (2004). "System reliability models for bridge structures." *Bulletin of the Polish academy of sciences*, 52(4), 321.

Nowak, A. S., and Collins, K. R. (2012). *Reliability of Structures*. CRC Press.

Ozgur, C. (2007). "Behaviour and Analysis of a Horizontally Curved and Skewed I-Girder Bridge." Georgia Institute of Technology.

Papadopoulos, V., Papadrakakis, M., and Deodatis, G. (2006). "Analysis of mean and mean square response of general linear stochastic finite element systems." *Computer Methods in Applied Mechanics and Engineering*, 195(41–43), 5454–5471.

Ren, J., Song, J., and Ellingwood, B. R. (2021). "Reliability assessment framework of deteriorating reinforced concrete bridges subjected to earthquake and pier scour." *Engineering Structures*, Elsevier Ltd, 239, 112363.

Road Research. (1979). *Evaluation of Load Carrying Capacity of Bridges*. Paris.

Saydam, D., and Frangopol, D. M. (2013). "Applicability of simple expressions for bridge system reliability assessment." *Computers and Structures*, Elsevier Ltd, 114–115, 59–71.

Shittu, A. (2015). "Probabilistic Evaluation of Horizontally Curved Aluminium Alloy Bridge Decks on Steel Girders." Ahmadu Bello University.

Shittu, A. A. (2020). "Structural reliability assessment of complex offshore structures based on non-intrusive stochastic methods." Cranfield University, Cranfield, UK.

Shittu, A. A., Kolios, A., and Mehmanparast, A. (2020a). "A Systematic Review of Structural Reliability Methods for Deformation and Fatigue Analysis of Offshore Jacket Structures." *Metals 2021, Vol. 11, Page 50*, Multidisciplinary Digital Publishing Institute, 11(1), 50.

Shittu, A. A., Mehmanparast, A., Amirafshari, P., Hart, P., and Kolios, A. (2020b). "Sensitivity analysis of design parameters for reliability assessment of offshore wind turbine jacket support structures." *Under review*.

Shittu, A. A., Mehmanparast, A., Hart, P., and Kolios, A. (2021). "Comparative study between S-N and fracture mechanics approach on reliability assessment of offshore wind turbine jacket foundations." *Reliability Engineering & System Safety*, Elsevier, 215, 107838.

Shittu, A. A., Mehmanparast, A., Shafiee, M., Kolios, A., Hart, P., and Pilario, K. (2020c). "Structural reliability assessment of offshore wind turbine support structures subjected to pitting corrosion-fatigue: A damage tolerance modelling approach." *Wind Energy*, John Wiley & Sons, Ltd, 23(11), 2004–2026.

Shittu, A. A., Mehmanparast, A., Wang, L., Salonitis, K., and Kolios, A. (2020d). "Comparative Study of Structural Reliability Assessment Methods for Offshore Wind Turbine Jacket Support Structures." *Applied Sciences (Switzerland)*, MDPI AG, 10(3).

Siwowski, T. (2006a). "Aluminium Bridges – Past, Present and Future." *Structural Engineering International Reports*, 286–293.

Siwowski, T. (2006b). "Aluminium bridges - Past, present and future." *Structural Engineering International: Journal of the International Association for Bridge and Structural Engineering (IABSE)*, Taylor & Francis, 16(4), 286–293.

Siwowski, T. (2009a). "FEM modelling and analysis of a certain aluminium bridge deck panel." *Archives of civil engineering*, LV. 3.

Siwowski, T. W. (2009b). "Structural behaviour of aluminium bridge deck panels." *Engineering Structures*, Elsevier, 31(7), 1349–1353.

Sorensen, J. D. (2003). *Note 1&2: Structural Reliability*. Aalborg, Denmark.

Thanapol, Y., Akiyama, M., and Frangopol, D. M. (2016). "Updating the Seismic Reliability of Existing RC Structures in a Marine Environment by Incorporating the Spatial Steel Corrosion Distribution: Application to Bridge Piers." *Journal of Bridge Engineering*, 21(7), 1–17.

Timoshenko, S. P., and Woinowsky-Krieger, S. (1982). *Theory of Plates and Shells*. McGraw Hill, London, UK.

Tindall, P. (2008). "Aluminium in Bridges." *ICE manual of Bridge Engineering*, Thomas Telford Ltd., London, UK.

Wang, C., Li, Q., and Ellingwood, B. R. (2016a). "Time-dependent reliability of ageing structures: an approximate approach." *Structure and Infrastructure Engineering*, Taylor & Francis, 12(12), 1566–1572.

Wang, L., and Kolios, A. (2017). "A generic framework for reliability assessment of offshore wind turbine monopiles considering soil-solid interaction and harsh marine environments." *Progress in the Analysis and Design of Marine Structures - Proceedings of the 6th International Conference on Marine Structures, MARSTRUCT 2017*, Lisbon, 931–938.

Wang, L., Kolios, A., Delafin, P.-L., Nishino, T., and Bird, T. (2015). "Fluid structure interaction modelling of a novel 10MW vertical-axis wind turbine rotor based on computational fluid dynamics and finite element analysis." *European Wind Energy Association Annual Conference and Exhibition 2015, EWEA 2015 - Scientific Proceedings*, 44(0).

Wang, L., Kolios, A., Nishino, T., Delafin, P. L., and Bird, T. (2016b). "Structural optimisation of vertical-axis wind turbine composite blades based on finite element analysis and genetic algorithm." *Composite Structures*, Elsevier Ltd, 153(January 2015), 123–138.

Wang, L., Quant, R., and Kolios, A. (2016c). "Fluid structure interaction modelling of horizontal-axis wind turbine blades based on CFD and FEA." *Journal of Wind Engineering and Industrial Aerodynamics*, Elsevier, 158, 11–25.

Wang, N., and Ellingwood, B. R. (2015). "Limit state design criteria for FRP strengthening of RC bridge components." *Structural Safety*, Elsevier Ltd, 56, 1–8.

Wang, N., Ellingwood, B. R., and Zureick, A. H. (2011a). "Bridge rating using system reliability assessment. II: Improvements to bridge rating practices." *Journal of Bridge Engineering*, 16(6), 863–871.

Wang, N., O'Malley, C., Ellingwood, B. R., and Zureick, A. H. (2011b). "Bridge rating using system reliability assessment. I: Assessment and verification by load testing." *Journal of Bridge Engineering*, 16(6), 854–862.

Webster, S. E., and Bannister, A. C. (2001). *Methods, Applications and Software for Structural Reliability Assessment*. Corus UK limited.

Yanweerasak, T., Pansuk, W., Akiyama, M., and Frangopol, D. M. (2018). "Life-cycle reliability assessment of reinforced concrete bridges under multiple hazards." *Structure and Infrastructure Engineering*, Taylor & Francis, 14(7), 1011–1024.

Zureick, A., and Naqib, R. (1999). "Horizontally Curved Steel I-Girders State-of-the-Art Analysis Methods." *Journal of Bridge Engineering*, American Society of Civil Engineers (ASCE), 4(1), 38–47.